

Is excess smoothing of Planck CMB anisotropy data partially responsible for evidence for dark energy dynamics in other $w(z)$ CDM parametrizations?

Chan-Gyung Park *

*Division of Science Education and Institute of Fusion Science,
Jeonbuk National University, Jeonju 54896, Republic of Korea*

Bharat Ratra †

Department of Physics, Kansas State University, 116 Cardwell Hall, Manhattan, KS 66506, USA

(Dated: January 8, 2025)

We study spatially-flat dynamical dark energy parametrizations, $w(z)$ CDM, with redshift-dependent dark energy equation of state parameter $w(z)$ expressed using three different quadratic and other polynomial forms (as functions of $1 - a$, where a is the scale factor), without and with a varying cosmic microwave background (CMB) lensing consistency parameter A_L . We use Planck CMB anisotropy data (P18 and lensing) and a large, mutually-consistent non-CMB data compilation that includes Pantheon+ type Ia supernova, baryon acoustic oscillation (BAO), Hubble parameter ($H(z)$), and growth factor ($f\sigma_8$) measurements, but not recent DESI BAO data. The six $w(z)$ CDM ($+A_L$) parametrizations show higher consistency between the CMB and non-CMB data constraints compared to the Λ CDM ($+A_L$) and w_0w_a CDM ($+A_L$) cases. Constraints from the most-restrictive P18+lensing+non-CMB data compilation on the six $w(z)$ CDM ($+A_L$) parametrizations indicate that dark energy dynamics is favored over a cosmological constant by $\gtrsim 2\sigma$ when $A_L = 1$, but only by $\gtrsim 1\sigma$ when A_L is allowed to vary (and $A_L > 1$ at $\sim 2\sigma$ significance). Non-CMB data dominate the P18+lensing+non-CMB compilation at low z and favor quintessence-like dark energy. At high z P18+lensing data dominate, favoring phantom-like dark energy with significance from 1.5σ to 2.9σ when $A_L = 1$, and from 1.1σ to 1.8σ when A_L varies. These results suggest that the observed excess weak lensing smoothing of some of the Planck CMB anisotropy multipoles is partially responsible for the $A_L = 1$ cases $\gtrsim 2\sigma$ evidence for dark energy dynamics over a cosmological constant.

PACS numbers: 98.80.-k, 95.36.+x

I. INTRODUCTION

In the standard spatially-flat Λ CDM cosmological model, [1], dark energy in the form of a cosmological constant Λ dominates the current cosmological energy budget and is responsible for the observed, low-redshift, accelerated cosmological expansion, with cold dark matter (CDM) being the next largest contributor to the current energy budget. This flat Λ CDM model agrees with many of the observational constraints, but there are some clouds, for recent reviews see [2–5].

A recent example is the DESI Collaboration result [6] determined from observational data analyzed in the spatially-flat w_0w_a CDM parametrization in which dynamical dark energy is taken to be a fluid with a parameterized equation of state parameter (the ratio of the fluid pressure to the fluid energy density) $w(a) = w_0 + w_a(1 - a) = w_0 + w_az/(1 + z) = w(z)$, a function of redshift z or cosmological scale factor a , [7, 8]. The analysis of new DESI baryon acoustic oscillation (BAO) measurements in combination with cosmic microwave background (CMB) data and Type Ia supernova (SNIa) observations, in particular the DESI+CMB+PantheonPlus

data compilation, see [6] for a detailed description, indicates that these data favor a region in parameter space that is $\gtrsim 2\sigma$ away from the flat Λ CDM model point at $w_0 = -1$ and $w_a = 0$, [6], thus indicating $\gtrsim 2\sigma$ support for dynamical dark energy over a cosmological constant. For discussions of the DESI result, see [9–57] and references therein.

In the w_0w_a CDM parametrization the $\gtrsim 2\sigma$ support for dynamical dark energy over a cosmological constant does not require including DESI BAO measurements or SNIa data in the analysis, [19]. A large compilation of independent, mutually-consistent, non-CMB measurements [58] used jointly with Planck CMB anisotropy data [59] provide slightly more restrictive constraints and support for dark energy dynamics, [19], than found from the DESI+CM+PantheonPlus compilation, [6]. And there have been earlier suggestions that dynamical dark energy is mildly favored over a cosmological constant, see [60–74] and references therein.

While the $\gtrsim 2\sigma$ support for dark energy dynamics in the w_0w_a CDM parametrization does not require using DESI BAO data or SNIa data in the analysis [19], part of this support seems to be related to the observed excess weak lensing smoothing of some Planck CMB anisotropy multipoles (relative to what is predicted in the Planck best-fit cosmological model), [59, 75], as follows, [50]. Including the lensing consistency parameter A_L [75] in the analysis, as a new free parameter to be determined from

* park.chan.gyung@gmail.com

† ratra@phys.ksu.edu

the dataset being analyzed, allows for a consistency check on the excess weak lensing smoothing. If the dataset under analysis gives a value of A_L that is consistent with unity then there is no excess smoothing. In the standard flat Λ CDM model, Planck CMB anisotropy data give $A_L > 1$ at $\sim 2\sigma$, indicating that there is excess smoothing [59, 76]. Including a varying A_L in an analysis of Planck CMB data and non-CMB data in the w_0w_a CDM+ A_L parametrization [50]: makes the Planck CMB data constraints and the non-CMB data constraints more consistent; again results in an $A_L > 1$ at $\sim 2\sigma$; and, reduces the support for dark energy dynamics over a cosmological constant to $\gtrsim 1\sigma$, compared to the $A_L = 1$ case support of $\gtrsim 2\sigma$, thus suggesting that the observed excess smoothing of some Planck CMB anisotropy multipoles contributes to the $\gtrsim 2\sigma$ support for dark energy dynamics in the $A_L = 1$ w_0w_a CDM parametrization.

In this study we extend earlier work [19, 50] by exploring three new spatially-flat $w(z)$ CDM (+ A_L) dynamical dark energy parametrizations with $w(z)$ expressed in quadratic and other polynomial forms as a function of $1 - a$. Utilizing the largest independent and mutually-consistent compilation of non-CMB data to date [58] together with Planck CMB data, we study these parametrizations to address the important question of whether dark energy exhibits dynamics beyond the cosmological constant. Through a combined analysis of the CMB (P18 and lensing) and non-CMB data compilation, we observationally constrain these dynamical dark energy parametrizations (without and with a varying CMB lensing consistency parameter A_L) and quantitatively investigate how well they fit the observations and how consistent the CMB and non-CMB data constraints are with each other in a given parametrization. We find from results of the analyses of the six $w(z)$ CDM (+ A_L) parametrizations (including $A_L = 1$ and varying A_L cases) that there is better consistency between the CMB and non-CMB data constraints than in the simpler XCDM (+ A_L) parametrizations with constant dark energy equation of state and in the w_0w_a CDM (+ A_L) parametrizations. In all six cases, the best-fit dark energy is dynamical and has quintessence-like behavior at low z and phantom-like behavior at high z . In the $A_L = 1$ cases dark energy dynamics is favored over a cosmological constant at $\gtrsim 2\sigma$, however in the varying A_L cases this support reduces to $\gtrsim 1\sigma$ (with $A_L > 1$ at $\sim 2\sigma$). This again suggests that the observed excess smoothing of some Planck CMB anisotropy multipoles contributes to the $\gtrsim 2\sigma$ support for dark energy dynamics in the three new $A_L = 1$ $w(z)$ CDM parametrizations we study here, consistent with the w_0w_a CDM(+ A_L) findings of [50].

In Sec. II we provide brief details of the data sets we use to constrain cosmological parameters in, and test the performance of, the flat $w(z)$ CDM parametrizations. In Sec. III we briefly summarize the main features of the three flat w_0w_2 CDM, w_0w_p CDM, and $w_0w_1w_2$ CDM parametrizations we study and the analysis techniques we use. Our results are presented and discussed in Sec. IV,

and we conclude in Sec. V.

II. DATA

In this paper CMB and non-CMB data sets are used to constrain the parameters of dynamical dark energy parameterizations. The data sets we use for this purpose are described in detail in Sec. II of [58] and outlined in what follows. We account for all known data covariances.

For the CMB data, we use the Planck 2018 TT,TE,EE+lowE (P18) CMB temperature and polarization power spectra alone as well as jointly with the Planck lensing potential (lensing) power spectrum [59, 77].

The non-CMB data set we use is the non-CMB (new) data compilation of [58], which is comprised of

- 16 BAO data points, spanning $0.122 \leq z \leq 2.334$, listed in Table I of [58]. We do not use DESI 2024 BAO data, [6].
- A 1590 SNIa data point subset of the Pantheon+ compilation [78], retaining only SNIa with $z > 0.01$ to mitigate peculiar velocity correction effects. These data span $0.01016 \leq z \leq 2.26137$,
- 32 Hubble parameter [$H(z)$] measurements, spanning $0.070 \leq z \leq 1.965$, listed in Table 1 of [79] and in Table II of [58].
- An additional nine (non-BAO) growth rate ($f\sigma_8$) data points, spanning $0.013 \leq z \leq 1.36$, listed in Table III of [58].

We use five individual and combined data sets to constrain the flat $w(z)$ CDM models with three different dark energy equation of state parameterizations: P18 data, P18+lensing data, non-CMB data, P18+non-CMB data, and P18+lensing+non-CMB data.

III. METHODS

Here we summarize the method we applied in this study. Additional details about the methodology we use are described in Sec. III of [58].

To determine quantitatively how restrictively these observational data constrain cosmological model parameters, we make use of the CAMB/COSMOMC program (October 2018 version) [80–82]. CAMB computes the evolution of spatial inhomogeneities and makes theoretical predictions which depend on the cosmological parameters of the dynamical dark energy parameterizations we study here. COSMOMC uses the Markov chain Monte Carlo (MCMC) method to compare these theoretical model predictions to observational data, to determine cosmological parameter likelihoods. The MCMC chains are assumed to have converged when the Gelman and Rubin R statistic (provided by COSMOMC) satisfies $R - 1 < 0.01$. For each model and

data set, we use the converged MCMC chains, with the `GetDist` code [83], to compute the average values, confidence intervals, and likelihood distributions of model parameters.

To establish a baseline for comparison, we also study the spatially-flat Λ CDM model. The six primary cosmological parameters for this model are conventionally chosen to be the current value of the physical baryonic matter density parameter $\Omega_b h^2$, the current value of the physical cold dark matter density parameter $\Omega_c h^2$, the angular size of the sound horizon at recombination $100\theta_{\text{MC}}$, the optical depth to reionization τ , the scalar-type primordial perturbation power spectral index n_s , and the power spectrum amplitude $\ln(10^{10} A_s)$, where h is the Hubble constant in units of $100 \text{ km s}^{-1} \text{ Mpc}^{-1}$. We assume flat priors for these parameters, non-zero over: $0.005 \leq \Omega_b h^2 \leq 0.1$, $0.001 \leq \Omega_c h^2 \leq 0.99$, $0.5 \leq 100\theta_{\text{MC}} \leq 10$, $0.01 \leq \tau \leq 0.8$, $0.8 \leq n_s \leq 1.2$, and $1.61 \leq \ln(10^{10} A_s) \leq 3.91$. In the flat Λ CDM+ A_L model (and the $w(z)$ CDM+ A_L parametrizations), for the lensing consistency parameter A_L we adopt a flat prior non-zero over $0 \leq A_L \leq 10$.

In the $w_0 w_a$ CDM parameterization dynamical dark energy is assumed to be a fluid with an evolving equation of state parameter (fluid pressure to energy density ratio) $w(a) = w_0 + w_a(1 - a)$ as a function of scale factor a or equivalently $w(z) = w_0 + w_a z/(1 + z)$ as a function of redshift z , [7, 8]. Since this two parameter dynamical dark energy parameterization explores a specific dark energy equation of state parameter region, we also study an extended three parameter $w_0 w_1 w_2$ CDM parametrization that includes the quadratic term,

$$w(a) = w_0 + w_1(1 - a) + w_2(1 - a)^2. \quad (1)$$

When $w_2 = 0$ and with $w_1 = w_a$, this reduces to the $w_0 w_a$ CDM parameterization. (Higher order terms are also possible, [84], but current data do not as effectively constrain dynamical dark energy parametrizations with four or more free parameters.) We first explore the two parameter $w_0 w_2$ CDM case with $w_1 = 0$, and then the more general case where w_0 , w_1 , and w_2 all vary.

We also consider an extension of the quadratic ($w_1 = 0$) case to an arbitrary order p form, with the three parameter $w_0 w_p$ CDM parameterization,

$$w(a) = w_0 + w_p(1 - a)^p, \quad (2)$$

where the order p is an additional dark energy parameter, in addition to w_0 and w_p .

In all cases we consider here and in [19, 50], at low redshift these $w(z)$ CDM parametrizations behave like an XCDM parametrization with $w_0 = w(z = 0)$, while at high redshift they also behave like an XCDM parametrization but now with $w(z \rightarrow \infty) = w_0 + w_a$ (for $w_0 w_a$ CDM), $= w_0 + w_2$ (for $w_0 w_2$ CDM), $= w_0 + w_p$ (for $w_0 w_p$ CDM), and $= w_0 + w_1 + w_2$ (for $w_0 w_1 w_2$ CDM). Compared to XCDM, these two- and three-parameter $w(z)$ CDM parametrizations have more flexibility in fitting data, allowing $w(z = 0)$ to better fit low-redshift

non-CMB data while $w(z \rightarrow \infty)$ can now better accommodate high-redshift CMB data. To allow for dynamical dark energy parametrizations whose equation of state parameter crosses $w = -1$, the CAMB/COSMOMC option of the parametrized post-Friedmann dark energy model [85] is used.

For the dynamical dark energy equation of state parameters in the $w_0 w_a$ CDM model parameterization we adopt flat priors non-zero over $-3.0 \leq w_0 \leq 0.2$ and $-3 < w_a < 2$. For the $w_0 w_p$ CDM parameterization, we apply an additional flat prior for the p parameter non-zero over $0 \leq p \leq 4$ while the flat prior for w_p is non-zero over $-3 \leq w_p \leq 2$. In the $w_0 w_1 w_2$ CDM parameterization we adopt an additional flat prior non-zero over $-3 \leq w_2 \leq 2$ with w_1 having the same prior as w_a .

When we estimate parameters using non-CMB data, we fix the values of τ and n_s to those obtained from P18 data (since these parameters cannot be determined solely from non-CMB data) and constrain the other cosmological parameters.

Additionally, we also present constraints on three derived parameters: the Hubble constant H_0 , the current value of the non-relativistic matter density parameter Ω_m , and the amplitude of matter fluctuations σ_8 , that are determined from those on the primary parameters of the cosmological model. We also record the values of the sum of dark energy equation of state parameters to which $w(z)$ approaches at high z , in the different dynamical dark energy parametrizations we study: $w_0 + w_a$, $w_1 + w_2 + w_3$, $w_0 + w_2$, and $w_0 + w_p$. These are determined from the primary parameters of the corresponding dynamical dark energy parametrization.

All the $w(z)$ CDM parametrizations we study here, as well as the Λ CDM model, have flat spatial hypersurfaces and a tilted scalar-type primordial scalar-type energy density perturbation power spectrum

$$P_\delta(k) = A_s \left(\frac{k}{k_0} \right)^{n_s}, \quad (3)$$

where k is the wavenumber and n_s and A_s are the spectral index and the amplitude and the power spectrum at pivot scale $k_0 = 0.05 \text{ Mpc}^{-1}$. This power spectrum is sourced by zero-point quantum fluctuations during an early epoch of power-law inflation in a spatially-flat inflation model with a scalar field inflaton potential energy density that is an exponential function of the inflaton [86–88].

To quantify how relatively well each model fits the dataset under consideration, we use differences in the Akaike information criterion (ΔAIC) and deviance information criterion (ΔDIC) between the information criterion (IC) values for the $w(z)$ CDM parametrization under study and the Λ CDM model. See Sec. III of [58] for a fuller discussion. According to the Jeffreys' scale we use, when $-2 \leq \Delta\text{IC} < 0$ there is *weak* evidence in favor of the model under study, when $-6 \leq \Delta\text{IC} < -2$ there is *positive* evidence, when $-10 \leq \Delta\text{IC} < -6$ there is *strong*

TABLE I. Consistency check parameter $\log_{10}\mathcal{I}$ and tension parameters σ and p (%) for P18 vs. non-CMB datasets and P18+lensing vs. non-CMB datasets in the flat w_0w_2 CDM, w_0w_2 CDM+ A_L , w_0w_pp CDM, w_0w_pp CDM+ A_L , $w_0w_1w_2$ CDM, and $w_0w_1w_2$ CDM+ A_L models.

Data	Flat w_0w_2 CDM model		Flat w_0w_2 CDM+ A_L model	
	P18 vs non-CMB	P18+lensing vs non-CMB	P18 vs non-CMB	P18+lensing vs non-CMB
$\log_{10}\mathcal{I}$	-0.605	-0.496	0.202	0.186
σ	2.538	2.462	1.833	1.851
p (%)	1.114	1.381	6.685	6.412
Data	Flat w_0w_pp CDM model		Flat w_0w_pp CDM+ A_L model	
	P18 vs non-CMB	P18+lensing vs non-CMB	P18 vs non-CMB	P18+lensing vs non-CMB
$\log_{10}\mathcal{I}$	-0.411	-0.308	0.344	0.358
σ	2.461	2.315	1.678	1.842
p (%)	1.386	2.064	9.341	6.545
Data	Flat $w_0w_1w_2$ CDM model		Flat $w_0w_1w_2$ CDM+ A_L model	
	P18 vs non-CMB	P18+lensing vs non-CMB	P18 vs non-CMB	P18+lensing vs non-CMB
$\log_{10}\mathcal{I}$	-0.609	-0.649	0.431	0.231
σ	2.615	2.589	1.872	1.901
p (%)	0.894	0.964	6.124	5.727

evidence, and when $\Delta\text{IC} < -10$ there is *very strong* evidence in favor of the model under study relative to the tilted flat Λ CDM model. This scale also holds when ΔIC is positive, but then the flat Λ CDM model is favored over the $w(z)$ CDM parametrization under study.

To quantitatively compare how consistent the cosmological parameter constraints (for the same parametrization) derived from two different data sets are, we use two estimators. The first is the DIC based $\log_{10}\mathcal{I}$, see [89] and Sec. III of [58]. When the two data sets are consistent $\log_{10}\mathcal{I} > 0$ while $\log_{10}\mathcal{I} < 0$ means that the two data sets are inconsistent. According to the Jeffreys' scale we use, the degree of consistency or inconsistency between two data sets is *substantial* if $|\log_{10}\mathcal{I}| > 0.5$, *strong* if $|\log_{10}\mathcal{I}| > 1$, and *decisive* if $|\log_{10}\mathcal{I}| > 2$, [89]. The second estimator is the tension probability p and the related, Gaussian approximation, "sigma value" σ , see [90–92] and Sec. III of [58]. $p = 0.05$ and $p = 0.003$ correspond to 2σ and 3σ Gaussian standard deviation, respectively.

IV. RESULTS AND DISCUSSION

Table I lists the values of the two statistical estimators, $\log_{10}\mathcal{I}$ and p values, that measure the consistency between cosmological parameter constraints from P18 and non-CMB data and from P18+lensing and non-CMB

data, for the three pairs of $w(z)$ CDM and $w(z)$ CDM+ A_L parametrizations we study in this paper. Compared to the corresponding values of the two statistical estimators in the w_0w_a CDM and w_0w_a CDM+ A_L cases, [19, 50], the values here for all six parametrizations we study indicate better consistency between the pairs of dataset constraints. Patterns similar to those seen in [19, 50] for the w_0w_a CDM (+ A_L) parametrizations are also found here. Allowing A_L to vary increases the consistency between the pairs of dataset constraints, but even for the $A_L = 1$ cases the pairs of dataset constraints agree to better than 3σ . As these dataset constraints are consistent, in the following we mostly focus on results from the largest dataset, the P18+lensing+non-CMB one.

Tables II and III summarize the parameter constraints for the w_0w_2 CDM (+ A_L) parametrizations. The likelihood distributions of the cosmological parameters are shown in Figures 1–4, with just the w_0 , w_2 , and $w_0 + w_2$ panels shown in Figures 5 and 6. Tables IV and V summarize the parameter constraints for the w_0w_pp CDM (+ A_L) parametrizations. The likelihood distributions of the cosmological parameters are shown in Figure 7–10, with just the w_0 , w_p , p , and $w_0 + w_p$ panels shown in Figures 11 and 12. Tables VI and VII summarize the parameter constraints for the $w_0w_1w_2$ CDM (+ A_L) parametrizations. The likelihood distributions of the cosmological parameters are shown in Figure 13–16, with just the w_0 , w_1 , w_2 , and $w_0 + w_1 + w_2$ panels shown in

TABLE II. Mean and 68% (or 95%) confidence limits of flat w_0w_2 CDM model parameters from non-CMB, P18, P18+lensing, P18+non-CMB, and P18+lensing+non-CMB data. H_0 has units of $\text{km s}^{-1} \text{Mpc}^{-1}$. We also list the values of χ^2_{min} , DIC, and AIC and the differences with respect to the values in the flat Λ CDM model for the same dataset, denoted by $\Delta\chi^2_{\text{min}}$, Δ DIC, and Δ AIC, respectively.

Parameter	Non-CMB	P18	P18+lensing	P18+non-CMB	P18+lensing+non-CMB
$\Omega_b h^2$	$0.0311^{+0.0039}_{-0.0045}$	0.02240 ± 0.00015	0.02243 ± 0.00015	0.02243 ± 0.00014	0.02244 ± 0.00014
$\Omega_c h^2$	$0.1011^{+0.0065}_{-0.012}$	0.1199 ± 0.0014	0.1193 ± 0.0012	0.1192 ± 0.0011	0.11917 ± 0.00099
$100\theta_{\text{MC}}$	$1.0234^{+0.0092}_{-0.011}$	1.04094 ± 0.00031	1.04100 ± 0.00030	1.04098 ± 0.00030	1.04098 ± 0.00030
τ	0.0540	0.0540 ± 0.0079	0.0520 ± 0.0075	0.0523 ± 0.0078	0.0527 ± 0.0074
n_s	0.9655	0.9655 ± 0.0043	0.9668 ± 0.0042	0.9668 ± 0.0040	0.9668 ± 0.0038
$\ln(10^{10} A_s)$	$3.54 \pm 0.27 (> 3.04)$	3.043 ± 0.016	3.037 ± 0.015	3.038 ± 0.016	3.039 ± 0.014
w_0	-0.864 ± 0.040	$-1.46^{+0.21}_{-0.44}$	$-1.44^{+0.21}_{-0.45}$	-0.898 ± 0.041	-0.898 ± 0.040
w_2	$-0.01^{+0.63}_{-0.25}$	$-1.1 \pm 1.3 (< 1.24)$	$-1.0 \pm 1.3 (< 1.34)$	$-1.12^{+0.51}_{-0.42}$	$-1.12^{+0.50}_{-0.40}$
$w_0 + w_2$	$-0.88^{+0.62}_{-0.23}$	$-2.56^{+0.90}_{-1.5}$	$-2.5^{+1.0}_{-1.6}$	$-2.02^{+0.48}_{-0.39}$	$-2.02^{+0.47}_{-0.37}$
H_0	$69.8^{+2.2}_{-2.5}$	$85 \pm 10 (> 66.0)$	$85 \pm 10 (> 66.7)$	67.90 ± 0.64	67.94 ± 0.64
Ω_m	$0.2724^{+0.0095}_{-0.017}$	$0.207^{+0.014}_{-0.065}$	$0.208^{+0.015}_{-0.066}$	0.3087 ± 0.0063	0.3083 ± 0.0063
σ_8	$0.819^{+0.031}_{-0.027}$	$0.961^{+0.11}_{-0.045}$	$0.951^{+0.11}_{-0.045}$	0.812 ± 0.011	0.8125 ± 0.0091
χ^2_{min}	1457.50	2761.24	2770.45	4233.13	4241.78
$\Delta\chi^2_{\text{min}}$	-12.43	-4.56	-4.26	-7.11	-7.48
DIC	1470.99	2815.85	2824.55	4289.62	4297.81
Δ DIC	-7.12	-2.08	-1.90	-2.71	-3.39
AIC	1469.50	2819.24	2828.45	4291.13	4299.78
Δ AIC	-8.43	-0.56	-0.26	-3.11	-3.48

Figures 17 and 18. Tables II–VII also list the $\Delta\chi^2_{\text{min}}$, Δ AIC, and Δ DIC values.

As in the w_0w_a CDM ($+A_L$) cases [19, 50] the constraints on the $w(z)$ parameters, as well as on the derived parameters H_0 , Ω_m , and σ_8 , from P18 and from P18+lensing data are less restrictive than those from non-CMB data.

We first compare the cosmological parameter values determined from P18+lensing+non-CMB data for the eight-parameter w_0w_2 CDM and the nine-parameter w_0w_2 CDM+ A_L parametrizations that are listed in the last columns of Tables II and III. Differences in the values of the six primary parameters common to the flat Λ CDM model are smaller than 1σ : $\Omega_b h^2$ (-0.54σ), $\Omega_c h^2$ ($+0.82\sigma$), $100\theta_{\text{MC}}$ (-0.37σ), τ ($+0.42\sigma$), n_s (-0.67σ), and $\ln(10^{10} A_s)$ ($+0.64\sigma$). For the two equation of state parameters, for the w_0w_2 CDM parametrization we find $w_0 = -0.898 \pm 0.040$ and $w_2 = -1.12^{+0.50}_{-0.40}$ while for the w_0w_2 CDM+ A_L parametrization we have $w_0 = -0.908 \pm 0.040$ and $w_2 = -0.78^{+0.48}_{-0.39}$, with the difference between these pair of values being $+0.18\sigma$ and -0.54σ . For the high- z asymptotic value of $w(z)$, $w_0 + w_2$, we find for the w_0w_2 CDM parametrization $w_0 + w_2 = -2.02^{+0.47}_{-0.37}$ while for the w_0w_2 CDM+ A_L parametrization $w_0 + w_2 =$

$-1.69^{+0.45}_{-0.36}$, with a -0.56σ difference between the two results. For the derived parameters H_0 , Ω_m , and σ_8 , the differences are $+0.01\sigma$, $+0.28\sigma$, and $+1.03\sigma$, respectively.

We now compare the cosmological parameter values determined from P18+lensing+non-CMB data for the nine-parameter w_0w_p pCDM and the ten-parameter w_0w_p pCDM+ A_L parametrizations that are listed in the last columns of Tables IV and V. Differences in the values of the six primary parameters common to the flat Λ CDM model are smaller than 1σ : $\Omega_b h^2$ (-0.49σ), $\Omega_c h^2$ ($+0.80\sigma$), $100\theta_{\text{MC}}$ (-0.28σ), τ ($+0.43\sigma$), n_s (-0.60σ), and $\ln(10^{10} A_s)$ ($+0.61\sigma$). For the three equation of state parameters, for the w_0w_p pCDM parametrization we find $w_0 = -0.916^{+0.031}_{-0.045}$, $w_p = -1.73^{+0.48}_{-1.2}$, and $p = 2.86^{+1.1}_{-0.26}$ (> 1.31) while for the w_0w_p pCDM+ A_L parametrization we have $w_0 = -0.917^{+0.032}_{-0.042}$, $w_p = -1.34^{+1.1}_{-0.69}$, and $p = 2.8 \pm 0.9$ (> 1.01), with the difference between these triplets of values being $+0.02\sigma$, -0.46σ , and $+0.06\sigma$. For the high- z asymptotic value of $w(z)$, $w_0 + w_p$, we find for the w_0w_p pCDM parametrization $w_0 + w_p = -2.65^{+0.54}_{-1.1}$ while for the w_0w_p pCDM+ A_L parametrization $w_0 + w_p = -2.26^{+1.2}_{-0.63}$, with a -0.47σ difference between the two results. For the derived parameters H_0 , Ω_m , and σ_8 , the differences are $+0.01\sigma$,

TABLE III. Mean and 68% (or 95%) confidence limits of flat $w_0w_2\text{CDM}+A_L$ model parameters from non-CMB, P18, P18+lensing, P18+non-CMB, and P18+lensing+non-CMB data. H_0 has units of $\text{km s}^{-1} \text{Mpc}^{-1}$. We also list the values of χ^2_{min} , DIC, and AIC and the differences with respect to the values in the flat ΛCDM model for the same dataset, denoted by $\Delta\chi^2_{\text{min}}$, ΔDIC , and ΔAIC , respectively.

Parameter	Non-CMB	P18	P18+lensing	P18+non-CMB	P18+lensing+non-CMB
$\Omega_b h^2$	$0.0311^{+0.0039}_{-0.0045}$	0.02258 ± 0.00017	0.02250 ± 0.00017	0.02263 ± 0.00016	0.02255 ± 0.00015
$\Omega_c h^2$	$0.1011^{+0.0065}_{-0.012}$	0.1182 ± 0.0015	0.1184 ± 0.0015	0.1177 ± 0.0012	0.1179 ± 0.0012
$100\theta_{\text{MC}}$	$1.0234^{+0.0092}_{-0.011}$	1.04114 ± 0.00033	1.04108 ± 0.00032	1.04119 ± 0.00032	1.04114 ± 0.00031
τ	0.0540	0.0494 ± 0.0087	$0.0495^{+0.0085}_{-0.0073}$	$0.0481^{+0.0089}_{-0.0074}$	0.0480 ± 0.0083
n_s	0.9654	0.9706 ± 0.0049	0.9690 ± 0.0048	0.9718 ± 0.0044	0.9706 ± 0.0042
$\ln(10^{10} A_s)$	$3.54 \pm 0.27 (> 3.04)$	3.030 ± 0.018	$3.030^{+0.018}_{-0.016}$	$3.026^{+0.018}_{-0.015}$	3.025 ± 0.017
A_L	...	$1.164^{+0.064}_{-0.087}$	$1.046^{+0.040}_{-0.055}$	1.186 ± 0.066	1.072 ± 0.038
w_0	-0.864 ± 0.040	$-1.15^{+0.35}_{-0.65}$	$-1.28^{+0.27}_{-0.58}$	-0.909 ± 0.040	-0.908 ± 0.040
w_2	$-0.01^{+0.63}_{-0.25}$	$-1.0 \pm 1.3 (< 1.24)$	$-0.9 \pm 1.3 (< 1.35)$	$-0.73^{+0.48}_{-0.38}$	$-0.78^{+0.48}_{-0.39}$
$w_0 + w_2$	$-0.88^{+0.62}_{-0.23}$	$-2.1^{+1.4}_{-1.2}$	-2.2 ± 1.2	$-1.64^{+0.45}_{-0.35}$	$-1.69^{+0.45}_{-0.36}$
H_0	$69.8^{+2.2}_{-2.5}$	$77^{+20}_{-8} (> 53.4)$	$80 \pm 13 (> 57.6)$	67.96 ± 0.63	67.93 ± 0.63
Ω_m	$0.2724^{+0.0095}_{-0.017}$	$0.268^{+0.038}_{-0.013}$	$0.240^{+0.022}_{-0.099}$	0.3052 ± 0.0062	0.3058 ± 0.0062
σ_8	$0.819^{+0.031}_{-0.027}$	$0.868^{+0.16}_{-0.085}$	$0.901^{+0.15}_{-0.066}$	0.795 ± 0.012	0.797 ± 0.012
χ^2_{min}	1457.50	2755.88	2770.27	4222.49	4237.66
$\Delta\chi^2_{\text{min}}$	-12.43	-9.92	-4.44	-17.75	-11.60
DIC	1470.99	2813.08	2825.76	4283.13	4295.89
ΔDIC	-7.12	-4.85	-0.69	-9.20	-5.31
AIC	1469.50	2815.88	2830.27	4282.49	4297.66
ΔAIC	-8.43	-3.92	+1.56	-11.75	-5.60

+0.26 σ , and +0.96 σ , respectively.

We finally compare the cosmological parameter values determined from P18+lensing+non-CMB data for the nine-parameter $w_0w_1w_2\text{CDM}$ and the ten-parameter $w_0w_1w_2\text{CDM}+A_L$ parametrizations that are listed in the last columns of Tables VI and VII. Differences in the values of the six primary parameters common to the flat ΛCDM model are smaller than 1σ : $\Omega_b h^2$ (-0.49σ), $\Omega_c h^2$ ($+0.85\sigma$), $100\theta_{\text{MC}}$ (-0.33σ), τ ($+0.42\sigma$), n_s (-0.64σ), and $\ln(10^{10} A_s)$ ($+0.64\sigma$). For the three equation of state parameters, for the $w_0w_1w_2\text{CDM}$ parametrization we find $w_0 = -0.929^{+0.077}_{-0.095}$, $w_1 = 0.27^{+0.87}_{-0.45}$, and $w_2 = -1.5 \pm 1.1 (< 0.709)$ while for the $w_0w_1w_2\text{CDM}+A_L$ parametrization we have $w_0 = -0.943^{+0.083}_{-0.095}$, $w_1 = 0.31^{+0.94}_{-0.54}$, and $w_2 = -1.2 \pm 1.2 (< 1.08)$, with the difference between these triplets of values being $+0.11\sigma$, -0.04σ , and -0.18σ . For the high- z asymptotic value of $w(z)$, $w_0 + w_1 + w_2$, we find for the $w_0w_1w_2\text{CDM}$ parametrization $w_0 + w_1 + w_2 = -2.15^{+0.40}_{-0.71}$ while for the $w_0w_1w_2\text{CDM}+A_L$ parametrization $w_0 + w_1 + w_2 = -1.88^{+0.50}_{-0.79}$, with a -0.30σ difference between the two results. For the derived parameters H_0 , Ω_m , and σ_8 , the differences are -0.04σ , $+0.34\sigma$, and $+0.99\sigma$, respectively.

To assess how relatively-well these spatially-flat dynamical dark energy parametrizations do in fitting the P18+lensing+non-CMB dataset, we compare their DIC values, more precisely their ΔDIC values relative to the DIC value of the standard flat ΛCDM model. These ΔDIC values are listed in Tables II–VII here, with the flat $w_0w_a\text{CDM} (+A_L)$ values listed in tables 1 and 2 of [50], the flat $\text{XCDM}+A_L$ parametrization value listed in table XI of [58] (in the flat XCDM parametrization with $A_L = 1$ the P18+lensing and the non-CMB cosmological constraints are inconsistent at 3.6σ , ruling the parametrization out at this significance, see [58]), and the flat $\Lambda\text{CDM}+A_L$ value listed in table VII of [58]. There is *positive* evidence in favor of all models and parametrizations relative to the flat ΛCDM model, with the $w_0w_p\text{CDM}+A_L$ parametrization with $\Delta\text{DIC} = -5.60$ favored the most and the $w_0w_a\text{CDM}$ parametrization with $\Delta\text{DIC} = -2.45$ favored the least over the flat ΛCDM model.

We now investigate whether the largest data compilation we study, the P18+lensing+non-CMB dataset, provides model-independent cosmological parameter constraints by comparing these constraints in several

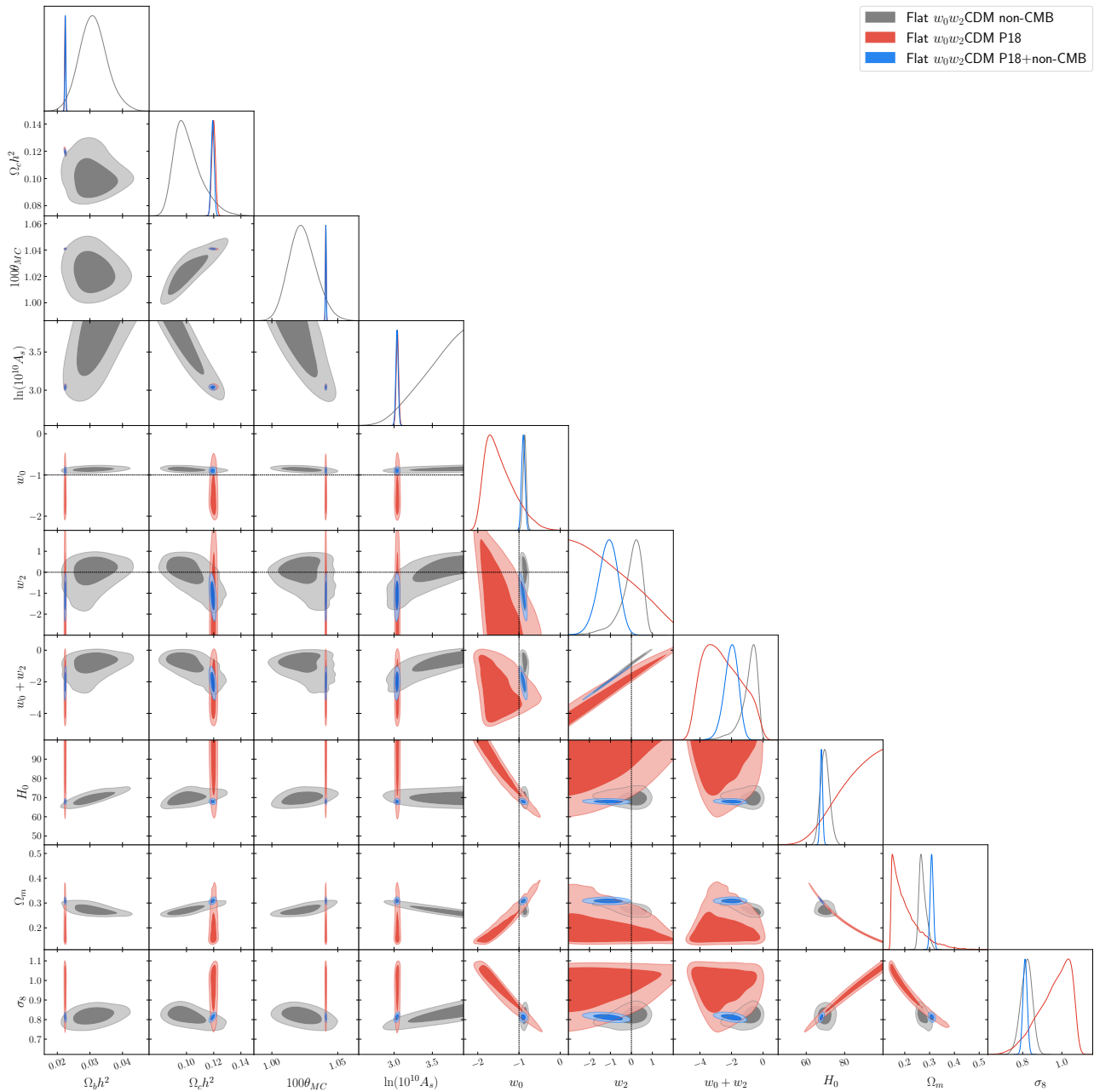


FIG. 1. One-dimensional likelihoods and 1σ and 2σ likelihood confidence contours of flat w_0w_2 CDM model parameters favored by non-CMB, P18, and P18+non-CMB datasets. We do not show τ and n_s , which are fixed in the non-CMB data analysis.

dark energy models and parametrizations. The P18+lensing+non-CMB data parameter constraints for the flat Λ CDM ($+A_L$) models are in tables IV and VII of [58], while those for the flat XCDM ($+A_L$) parametrization are in table XI there. In this analysis we do not consider the flat XCDM parametrization with $A_L = 1$ since P18+lensing constraints and non-CMB constraints are more than 3σ inconsistent in this case [58]. P18+lensing+non-CMB data parameter constraints for the flat w_0w_a CDM ($+A_L$) parametrizations are in table 1 and 2 of [50], while those of the flat w_0w_2 CDM

($+A_L$), w_0w_p CDM ($+A_L$), and $w_0w_1w_2$ CDM ($+A_L$) parametrizations are in Tables II –VII.

We first consider the $A_L = 1$ flat dark energy models and parametrizations and first compute the largest model-to-model differences for the six common model parameters. For $\Omega_b h^2$ the largest value is 0.02249 ± 0.00013 in the Λ CDM model and the smallest is 0.02244 ± 0.00014 in the w_0w_a CDM and w_0w_2 CDM parametrizations, resulting in a difference of 0.26σ . For $\Omega_c h^2$ the smallest value is 0.11849 ± 0.00084 in the Λ CDM model and the largest is 0.11917 ± 0.00099 in the

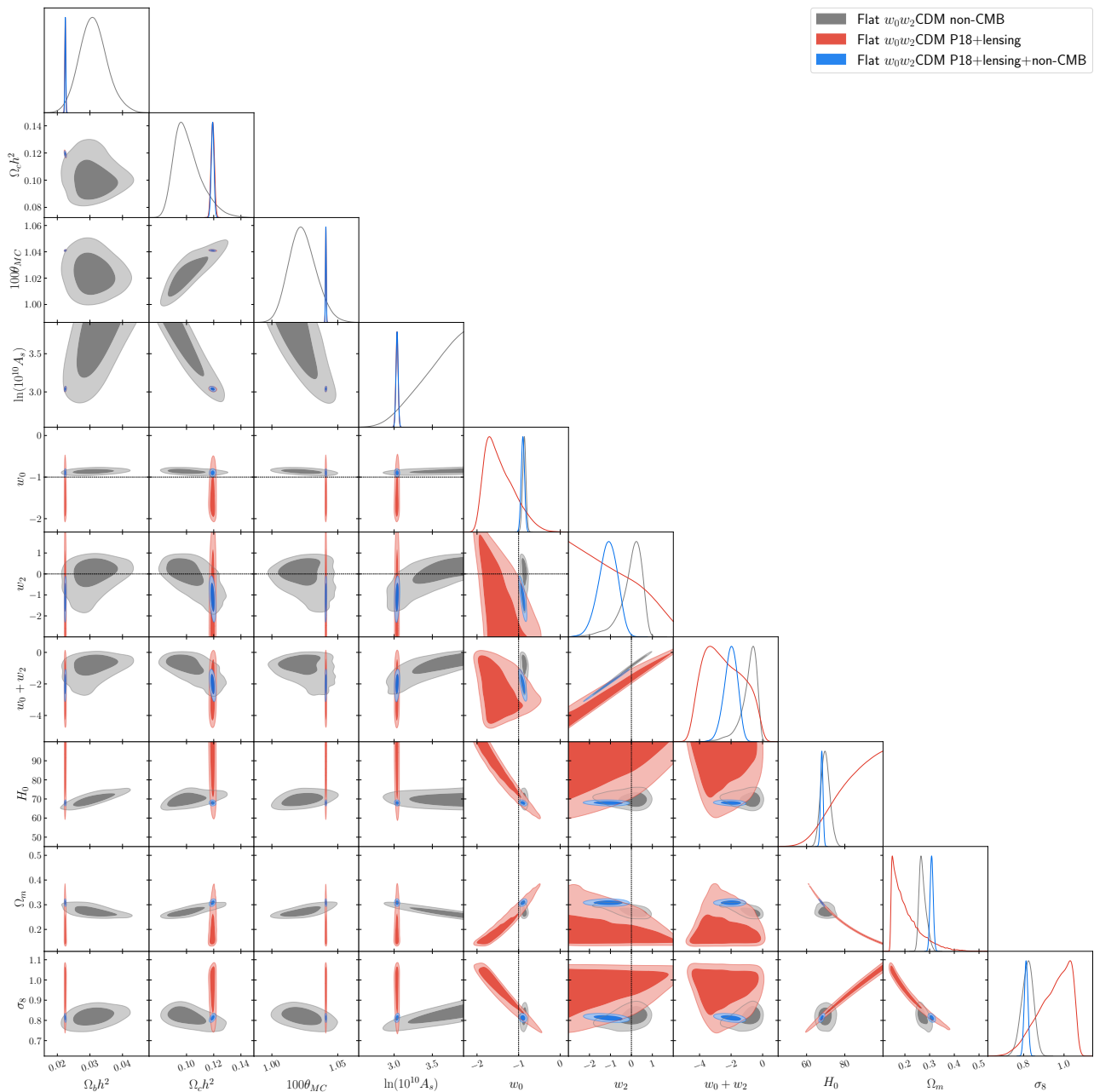


FIG. 2. One-dimensional likelihoods and 1σ and 2σ likelihood confidence contours of flat w_0w_2 CDM model parameters favored by non-CMB, P18+lensing, P18+lensing+non-CMB datasets. We do not show τ and n_s , which are fixed in the non-CMB data analysis.

w_0w_2 CDM parametrization, resulting in a difference of 0.52σ . For $100\theta_{MC}$ the Λ CDM model $100\theta_{MC} = 1.04109 \pm 0.00028$ is the largest and the w_0w_2 CDM parametrization $100\theta_{MC} = 1.04098 \pm 0.00030$ is the smallest, giving a difference of 0.27σ . For τ and n_s the largest deviation is 0.41σ and 0.32σ , respectively, between the largest Λ CDM model values ($\tau = 0.0569 \pm 0.0071$ and $n_s = 0.9685 \pm 0.0036$) and the smallest w_0w_2 CDM parametrization values ($\tau = 0.0527 \pm 0.0074$ and $n_s = 0.9668 \pm 0.0038$). For $\ln(10^{10} A_s)$ the Λ CDM

model largest value ($\ln(10^{10} A_s) = 3.046 \pm 0.014$) and the w_0w_2 CDM, w_0w_p pCDM, and $w_0w_1w_2$ CDM parametrizations smallest value ($\ln(10^{10} A_s) = 3.039 \pm 0.014$) differ by 0.35σ . Thus for $A_L = 1$ the six common model parameters agree between the various dark energy models and parametrizations to well within 1σ , and we expect the same for the derived parameters, as we now show. For the derived parameter H_0 , $68.05 \pm 0.38 \text{ km s}^{-1} \text{ Mpc}^{-1}$ in the Λ CDM model is the largest value and $67.80 \pm 0.64 \text{ km s}^{-1} \text{ Mpc}^{-1}$ in the w_0w_a CDM parametrization is the

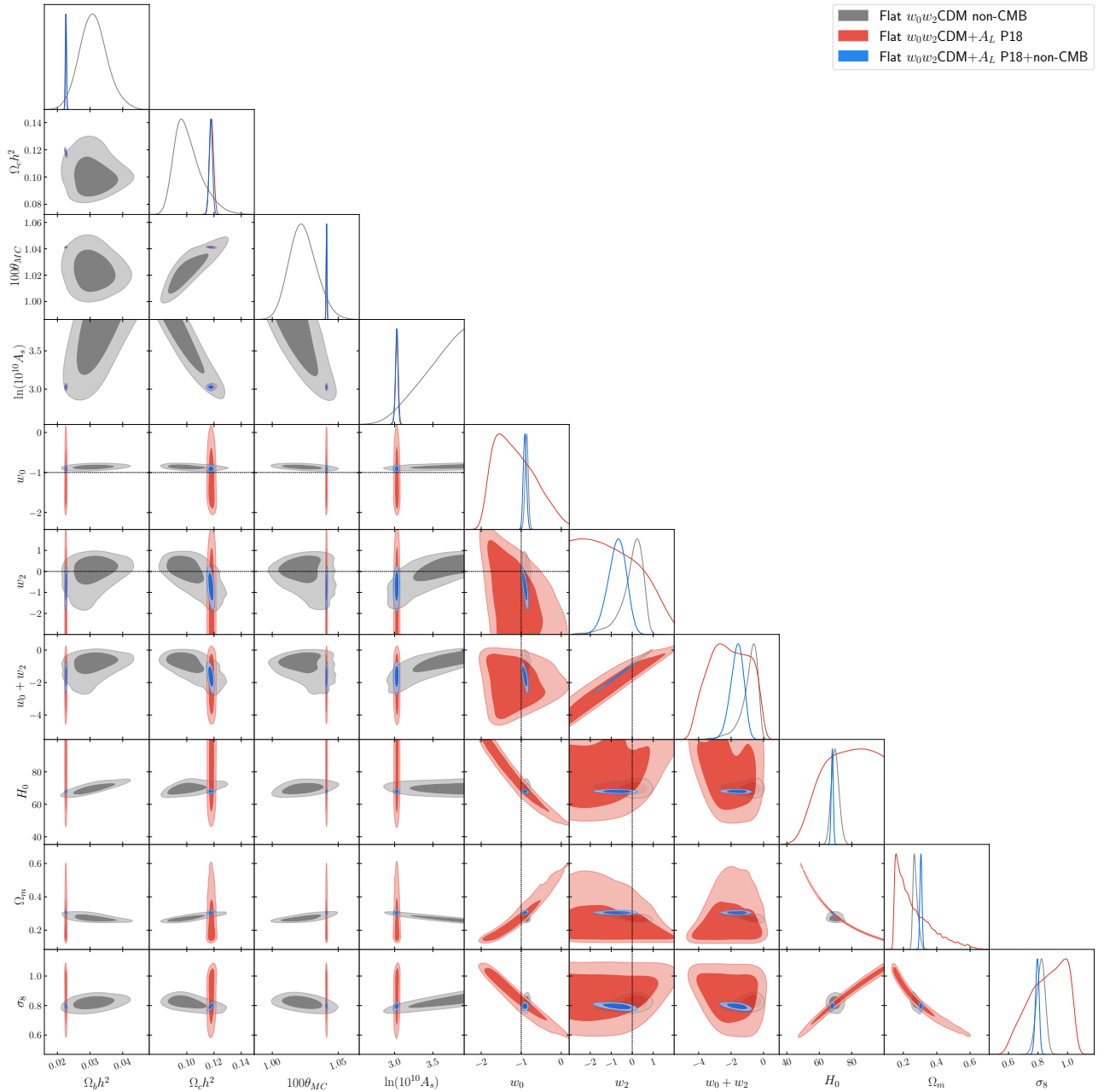


FIG. 3. One-dimensional likelihoods and 1σ and 2σ likelihood confidence contours of flat $w_0w_2\text{CDM}+A_L$ model parameters favored by non-CMB, P18, and P18+non-CMB datasets. We do not show τ and n_s , which are fixed in the non-CMB data analysis.

smallest, giving a difference of 0.34σ . The ΛCDM model has the smallest $\Omega_m = 0.3059 \pm 0.0050$ and the $w_0w_a\text{CDM}$ parametrization has the largest $\Omega_m = 0.3094 \pm 0.0063$ which differ from each other by 0.44σ while the ΛCDM model smallest $\sigma_8 = 0.8077 \pm 0.0057$ and the $w_0w_2\text{CDM}$ parametrization largest $\sigma_8 = 0.8125 \pm 0.0091$ differ by 0.45σ . In the $A_L = 1$ case the P18+lensing+non-CMB data compilation provides reasonably model-independent parameter constraints, with the largest difference being the 0.52σ for Ω_ch^2 .

For the A_L -varying dark energy models and parametrizations, where we include the $\text{XCDM}+A_L$ case, the largest model-to-model differences for the six common model parameters are as follows. For $\Omega_b h^2$ the largest is 0.02263 ± 0.00014 in the $\text{XCDM}+A_L$ parametrization and the smallest is 0.02255 ± 0.00015 in the $w_0w_2\text{CDM}+A_L$ or $w_0w_p\text{CDM}+A_L$ or $w_0w_1w_2\text{CDM}+A_L$ parametrization, resulting in a difference of 0.39σ . For Ω_ch^2 the smallest is 0.1168 ± 0.0011 in the $\text{XCDM}+A_L$ parametrization and the largest is

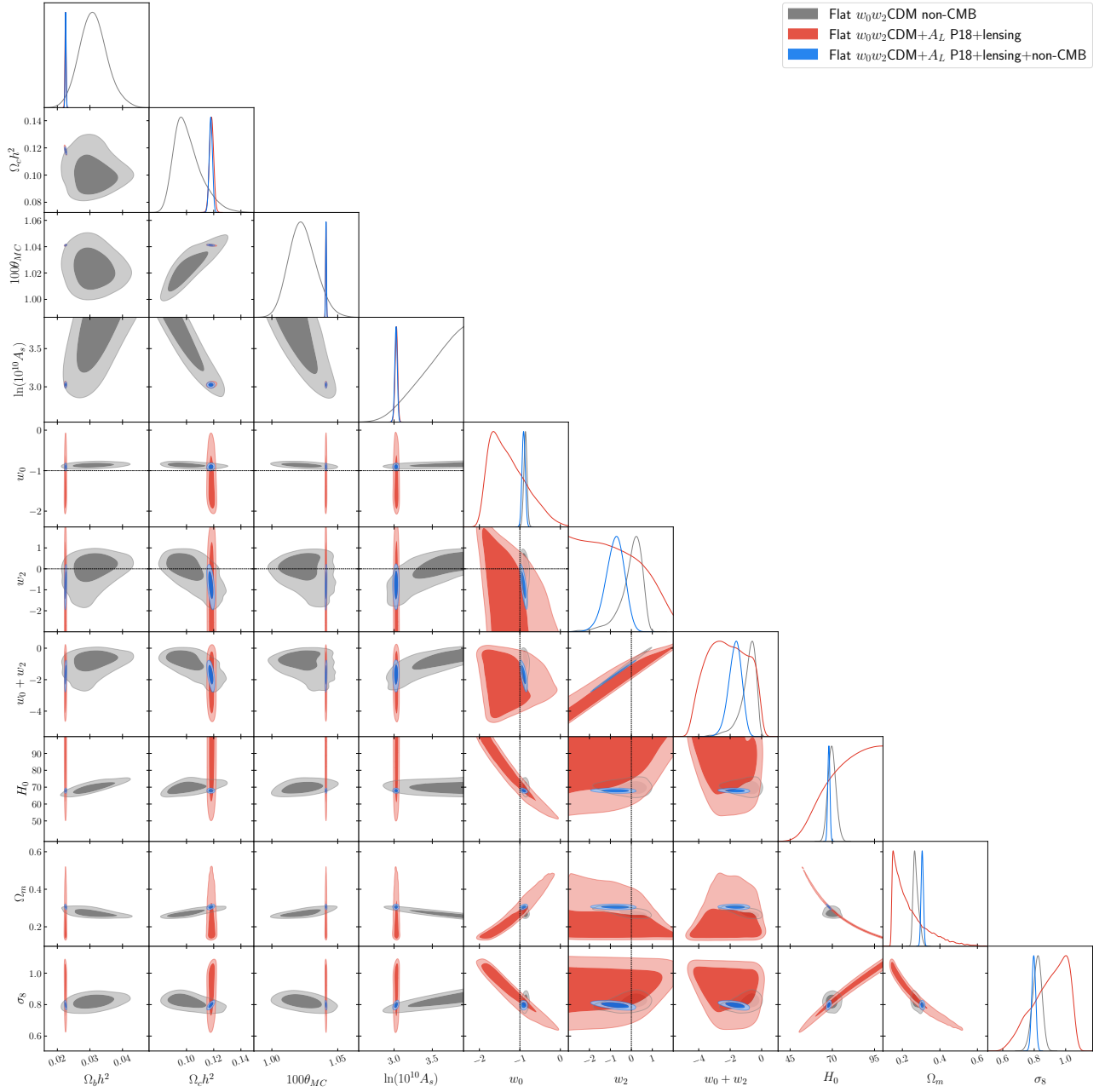


FIG. 4. One-dimensional likelihoods and 1σ and 2σ likelihood confidence contours of flat $w_0w_2\text{CDM}+A_L$ model parameters favored by non-CMB, P18+lensing, P18+lensing+non-CMB datasets. We do not show τ and n_s , which are fixed in the non-CMB data analysis.

0.1179 ± 0.0012 in the $w_0w_2\text{CDM}+A_L$ case, resulting in a difference of 0.68σ . For $100\theta_{MC}$, the $\Lambda\text{CDM}+A_L$ parametrization $100\theta_{MC} = 1.04126 \pm 0.00030$ is the largest and the $w_0w_p\text{CDM}+A_L$ or $w_0w_1w_2\text{CDM}+A_L$ case $100\theta_{MC} = 1.04113 \pm 0.00030$ is the smallest, giving a difference of 0.31σ . For τ the largest difference is 0.16σ between the $\Lambda\text{CDM}+A_L$ model smallest $\tau = 0.0477 \pm 0.0086$ and the $\Lambda\text{CDM}+A_L$ parametrization largest $\tau = 0.0496 \pm 0.0083$, while for n_s the largest difference is 0.48σ between the $\Lambda\text{CDM}+A_L$

parametrization largest $n_s = 0.9733 \pm 0.0040$ and the $w_0w_p\text{CDM}+A_L$ case smallest $n_s = 0.9705 \pm 0.0042$. For $\ln(10^{10}A_s)$, the $\Lambda\text{CDM}+A_L$ model smallest $\ln(10^{10}A_s) = 3.024 \pm 0.018$ and the $\Lambda\text{CDM}+A_L$ case largest $\ln(10^{10}A_s) = 3.026 \pm 0.017$ differ at 0.08σ . For the derived parameters, the largest $H_0 = 68.45 \pm 0.42 \text{ km s}^{-1} \text{ Mpc}^{-1}$ in the $\Lambda\text{CDM}+A_L$ model and the smallest $H_0 = 67.79 \pm 0.63 \text{ km s}^{-1} \text{ Mpc}^{-1}$ in the $\Lambda\text{CDM}+A_L$ case differ at 0.87σ . The $\Lambda\text{CDM}+A_L$ model smallest $\Omega_m = 0.3005 \pm 0.0053$ and the $w_0w_a\text{CDM}+A_L$ case

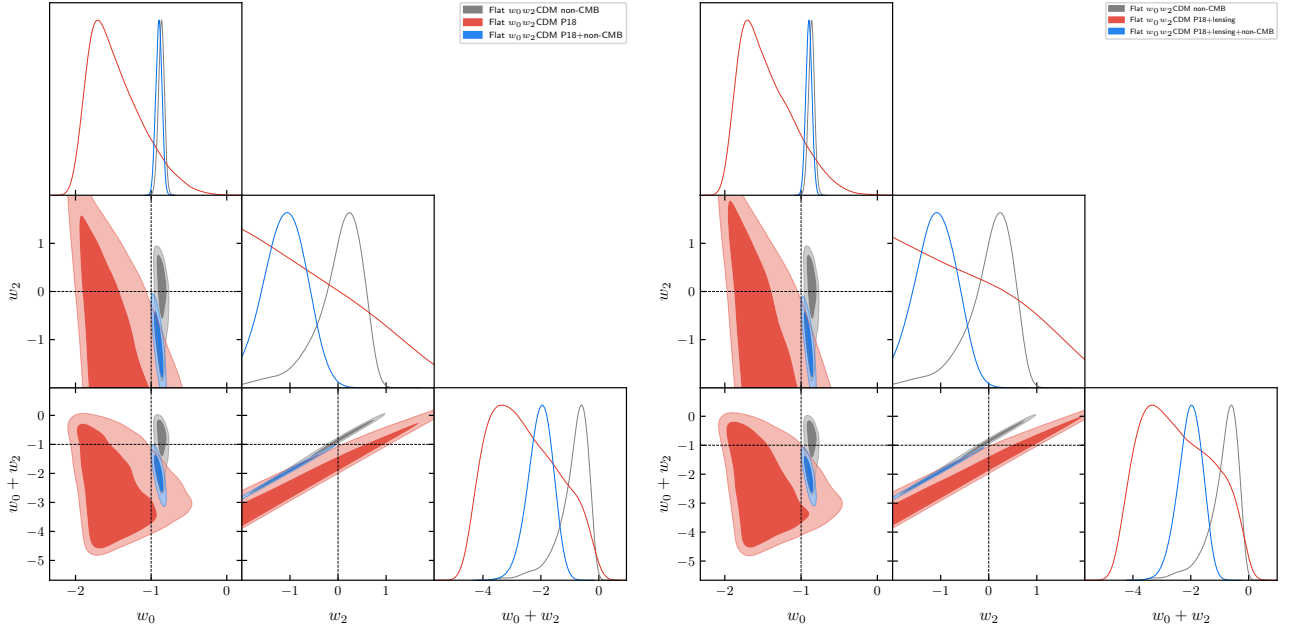


FIG. 5. One-dimensional likelihoods and 1σ and 2σ likelihood confidence contours of w_0 , w_2 , and $w_0 + w_2$ parameters in the flat w_0w_2 CDM parametrization favored by (left) non-CMB, P18, and P18+non-CMB datasets, and (right) non-CMB, P18+lensing, and P18+lensing+non-CMB datasets.

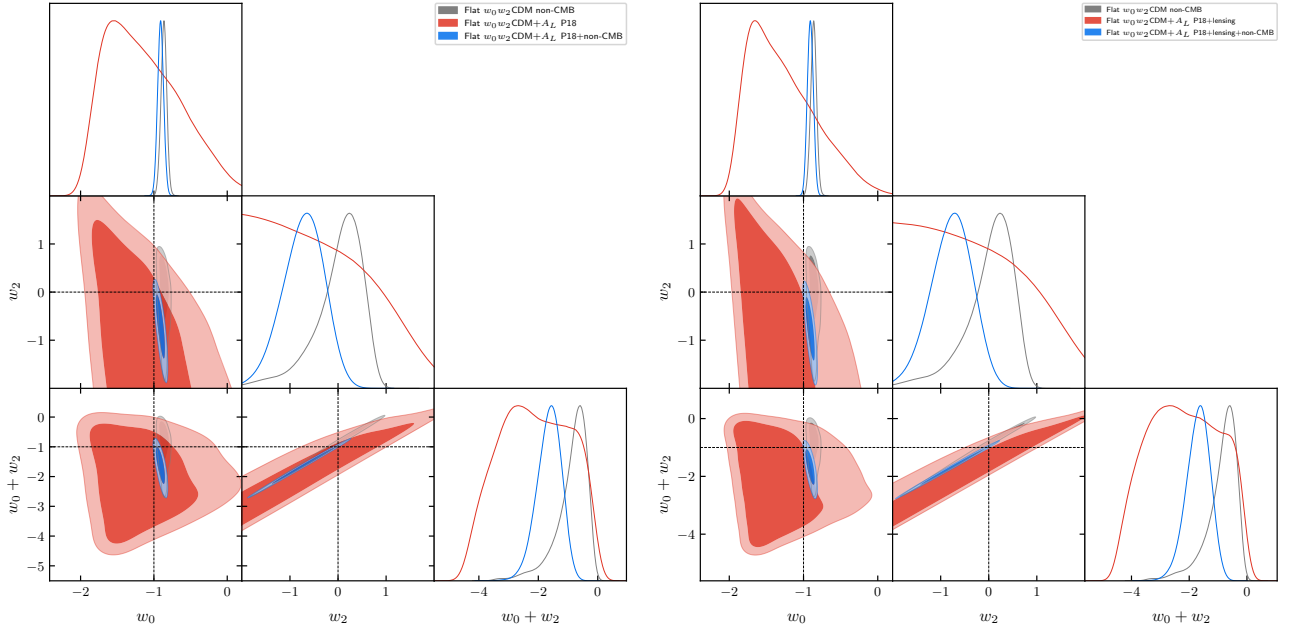


FIG. 6. One-dimensional likelihoods and 1σ and 2σ likelihood confidence contours of w_0 , w_2 , and $w_0 + w_2$ parameters in the flat w_0w_2 CDM+ A_L parametrization favored by (left) non-CMB, P18, and P18+non-CMB datasets, and (right) non-CMB, P18+lensing, and P18+lensing+non-CMB datasets.

largest $\Omega_m = 0.3062 \pm 0.0064$ differ by 0.69σ while the Λ CDM+ A_L model smallest $\sigma_8 = 0.785 \pm 0.011$ and the w_0w_2 CDM+ A_L or w_0w_p CDM or $w_0w_1w_2$ CDM parametrization largest $\sigma_8 = 0.797 \pm 0.012$ differ from each other by 0.74σ . The spread in parameter values

across dark energy models and parametrizations, when measured using P18+lensing+non-CMB data, is a little larger when A_L is allowed to vary, compared to the $A_L = 1$ case. Among the six common primary parameters, the biggest spread, 0.68σ , is again in

TABLE IV. Mean and 68% (or 95%) confidence limits of flat w_0w_p CDM model parameters from non-CMB, P18, P18+lensing, P18+non-CMB, and P18+lensing+non-CMB data. H_0 has units of $\text{km s}^{-1} \text{Mpc}^{-1}$. We also list the values of χ^2_{\min} , DIC, and AIC and the differences with respect to the values in the flat Λ CDM model for the same dataset, denoted by $\Delta\chi^2_{\min}$, Δ DIC, and Δ AIC, respectively.

Parameter	Non-CMB	P18	P18+lensing	P18+non-CMB	P18+lensing+non-CMB
$\Omega_b h^2$	0.0308 ± 0.0044	0.02239 ± 0.00015	0.02243 ± 0.00015	0.02245 ± 0.00014	0.02245 ± 0.00014
$\Omega_c h^2$	$0.1014^{+0.0073}_{-0.012}$	0.1199 ± 0.0014	0.1193 ± 0.0012	0.1191 ± 0.0011	0.11904 ± 0.00098
$100\theta_{\text{MC}}$	$1.0228^{+0.0097}_{-0.011}$	1.04094 ± 0.00031	1.04099 ± 0.00031	1.04100 ± 0.00030	1.04101 ± 0.00030
τ	0.0540	0.0540 ± 0.0079	0.0522 ± 0.0075	0.0527 ± 0.0077	0.0530 ± 0.0073
n_s	0.9655	0.9655 ± 0.0044	0.9667 ± 0.0041	0.9672 ± 0.0039	0.9671 ± 0.0038
$\ln(10^{10} A_s)$	$3.52 \pm 0.26 (> 3.06)$	3.044 ± 0.016	3.038 ± 0.015	3.038 ± 0.016	3.039 ± 0.014
w_0	$-0.865^{+0.048}_{-0.041}$	$-1.40^{+0.29}_{-0.55}$	$-1.39^{+0.26}_{-0.53}$	$-0.914^{+0.031}_{-0.046}$	$-0.916^{+0.031}_{-0.045}$
w_p	$-0.25^{+0.95}_{-0.23}$	$-1.0 \pm 1.3 (< 1.36)$	$-1.0 \pm 1.3 (< 1.35)$	$-1.70^{+0.52}_{-1.2}$	$-1.73^{+0.48}_{-1.2}$
p	$2.5 \pm 1.1 (> 0.454)$	$1.93^{+0.87}_{-1.7} (> 0.257)$	$2.0 \pm 1.1 (> 0.276)$	$2.8 \pm 0.8 (> 1.20)$	$2.86^{+1.1}_{-0.26} (> 1.31)$
$w_0 + w_p$	$-1.11^{+0.96}_{-0.19}$	$-2.4^{+1.1}_{-1.3}$	$-2.4^{+1.1}_{-1.3}$	$-2.61^{+0.54}_{-1.2}$	$-2.65^{+0.54}_{-1.1}$
H_0	69.7 ± 2.4	$86 \pm 10 (> 66.8)$	$85 \pm 10 (> 66.8)$	67.89 ± 0.63	67.92 ± 0.64
Ω_m	$0.273^{+0.011}_{-0.017}$	$0.205^{+0.013}_{-0.062}$	$0.205^{+0.014}_{-0.063}$	0.3086 ± 0.0063	0.3082 ± 0.0062
σ_8	$0.818^{+0.031}_{-0.027}$	$0.964^{+0.10}_{-0.045}$	$0.955^{+0.10}_{-0.042}$	0.811 ± 0.011	0.8114 ± 0.0091
χ^2_{\min}	1457.48	2761.04	2770.34	4231.80	4240.63
$\Delta\chi^2_{\min}$	-12.45	-4.76	-4.37	-8.44	-8.63
DIC	1471.29	2815.91	2824.51	4289.09	4297.22
Δ DIC	-6.82	-2.02	-1.94	-3.24	-3.98
AIC	1471.48	2821.04	2830.34	4291.80	4300.63
Δ AIC	-6.45	+1.24	+1.63	-2.44	-2.63

$\Omega_c h^2$, while the three derived parameters have larger spreads, ranging from 0.69σ to 0.87σ . Since these are all smaller than 1σ we conclude that even in the varying A_L case P18+lensing+non-CMB data provide reasonably model-independent cosmological parameter measurements.

For all the $A_L = 1$ and A_L -varying dark energy models and parametrizations together, but excluding the XCDM case with $A_L = 1$, the largest model-to-model differences for the six common model parameters are as follows. For $\Omega_b h^2$, the largest 0.02263 ± 0.00014 in the XCDM+ A_L case and the smallest 0.02244 ± 0.00014 in the w_0w_a CDM or w_0w_2 CDM parametrization have a difference of 0.96σ . For $\Omega_c h^2$ the smallest is 0.1168 ± 0.0011 in the XCDM+ A_L case and the largest is 0.11917 ± 0.00099 in the w_0w_2 CDM parametrization, resulting in a difference of 1.60σ . For $100\theta_{\text{MC}}$, the XCDM+ A_L case $100\theta_{\text{MC}} = 1.04126 \pm 0.00030$ is the largest and the w_0w_2 CDM parametrization $100\theta_{\text{MC}} = 1.04098 \pm 0.00030$ is the smallest, and these have a difference of 0.66σ . For τ the largest difference is 0.82σ between the Λ CDM model largest $\tau = 0.0569 \pm 0.0071$ and the XCDM+ A_L model smallest $\tau = 0.0477 \pm 0.0086$, while for n_s the largest

difference is 1.18σ between the XCDM+ A_L case largest $n_s = 0.9733 \pm 0.0040$ and the w_0w_2 CDM case smallest $n_s = 0.9668 \pm 0.0038$. For $\ln(10^{10} A_s)$, the Λ CDM model largest $\ln(10^{10} A_s) = 3.046 \pm 0.014$ and the XCDM+ A_L model smallest $\ln(10^{10} A_s) = 3.024 \pm 0.018$ differ at 0.96σ . For the derived parameters, the largest $H_0 = 68.45 \pm 0.42 \text{ km s}^{-1} \text{Mpc}^{-1}$ in the XCDM+ A_L model and the smallest $H_0 = 67.79 \pm 0.63 \text{ km s}^{-1} \text{Mpc}^{-1}$ in the XCDM+ A_L case differ by 0.87σ . The XCDM+ A_L model smallest $\Omega_m = 0.3005 \pm 0.0053$ and the w_0w_a CDM case largest $\Omega_m = 0.3094 \pm 0.0063$ have the largest difference of 1.08σ while the XCDM+ A_L case smallest $\sigma_8 = 0.785 \pm 0.011$ and the w_0w_2 CDM model parametrization largest $\sigma_8 = 0.8125 \pm 0.0091$ differ by 1.93σ . The parameter value differences are larger when we compare across all the $A_L = 1$ and varying A_L cases, caused by the somewhat significant changes in some parameter values when the lensing consistency parameter is allowed to vary, compared to the $A_L = 1$ case values.

As described above, the significance of the difference between the largest and smallest H_0 values are 0.34σ (when $A_L = 1$), 0.87σ (when A_L varies), and 0.87σ (overall), indicating that for these models P18+lensing+non-

TABLE V. Mean and 68% (or 95%) confidence limits of flat $w_0w_p p\text{CDM}+A_L$ model parameters from non-CMB, P18, P18+lensing, P18+non-CMB, and P18+lensing+non-CMB data. H_0 has units of $\text{km s}^{-1} \text{Mpc}^{-1}$. We also list the values of χ^2_{min} , DIC, and AIC and the differences with respect to the values in the flat ΛCDM model for the same dataset, denoted by $\Delta\chi^2_{\text{min}}$, ΔDIC , and ΔAIC , respectively.

Parameter	Non-CMB	P18	P18+lensing	P18+non-CMB	P18+lensing+non-CMB
$\Omega_b h^2$	0.0308 ± 0.0044	0.02258 ± 0.00017	0.02250 ± 0.00017	0.02263 ± 0.00015	0.02255 ± 0.00015
$\Omega_c h^2$	$0.1014^{+0.0073}_{-0.012}$	0.1182 ± 0.0015	0.1185 ± 0.0015	0.1177 ± 0.0012	0.1178 ± 0.0012
$100\theta_{\text{MC}}$	$1.0228^{+0.0097}_{-0.011}$	1.04113 ± 0.00032	1.04108 ± 0.00032	1.04118 ± 0.00031	1.04113 ± 0.00030
τ	0.0540	$0.0495^{+0.0089}_{-0.0077}$	$0.0494^{+0.0087}_{-0.0074}$	$0.0481^{+0.0088}_{-0.0074}$	$0.0481^{+0.0087}_{-0.0073}$
n_s	0.9655	0.9705 ± 0.0049	0.9690 ± 0.0048	0.9718 ± 0.0043	0.9705 ± 0.0042
$\ln(10^{10} A_s)$	$3.52 \pm 0.26 (> 3.06)$	$3.030^{+0.019}_{-0.016}$	$3.029^{+0.019}_{-0.016}$	$3.026^{+0.018}_{-0.015}$	$3.025^{+0.018}_{-0.015}$
A_L	...	$1.165^{+0.063}_{-0.088}$	$1.047^{+0.039}_{-0.058}$	1.184 ± 0.064	1.072 ± 0.038
w_0	$-0.865^{+0.048}_{-0.041}$	$-1.16^{+0.44}_{-0.66}$	$-1.24^{+0.37}_{-0.63}$	$-0.916^{+0.032}_{-0.043}$	$-0.917^{+0.032}_{-0.042}$
w_p	$-0.25^{+0.95}_{-0.23}$	$-0.81^{+0.82}_{-2.1}$	$-0.8 \pm 1.3 (< 1.41)$	$-1.29^{+1.1}_{-0.69}$	$-1.34^{+1.1}_{-0.69}$
p	$2.5 \pm 1.1 (> 0.454)$	$2.0^{+1.3}_{-1.5}$	$2.0 \pm 1.1 (> 0.269)$	$2.8 \pm 0.9 (> 0.980)$	$2.8 \pm 0.9 (> 1.01)$
$w_0 + w_p$	$-1.11^{+0.96}_{-0.19}$	$-1.97^{+1.5}_{-0.95}$	$-2.0^{+1.4}_{-1.1}$	$-2.20^{+1.1}_{-0.62}$	$-2.26^{+1.2}_{-0.63}$
H_0	69.7 ± 2.4	$77^{+20}_{-8} (> 54.7)$	$80 \pm 13 (> 57.7)$	67.94 ± 0.65	67.91 ± 0.64
Ω_m	$0.273^{+0.011}_{-0.017}$	$0.261^{+0.030}_{-0.012}$	$0.241^{+0.023}_{-0.10}$	0.3054 ± 0.0063	0.3059 ± 0.0063
σ_8	$0.818^{+0.031}_{-0.027}$	$0.874^{+0.16}_{-0.080}$	$0.899^{+0.15}_{-0.067}$	0.795 ± 0.012	0.797 ± 0.012
χ^2_{min}	1457.48	2755.89	2770.20	4221.77	4237.05
$\Delta\chi^2_{\text{min}}$	-12.45	-9.91	-4.51	-18.47	-12.21
DIC	1471.29	2812.89	2825.96	4282.60	4295.60
ΔDIC	-6.82	-5.04	-0.49	-9.73	-5.60
AIC	1471.48	2817.89	2832.20	4282.60	4299.05
ΔAIC	-6.45	-1.91	+3.50	-10.47	-4.21

CMB data provide a reasonably model-independent H_0 value, which may be summarized as $H_0 = 68.1 \pm 0.9 \text{ km s}^{-1} \text{Mpc}^{-1}$, where the central value is the average of the smallest and largest values and the error bar is half of the spread between the largest upper 1σ value and the smallest lower 1σ value. This summary values agrees with the median statistics result $H_0 = 68 \pm 2.8 \text{ km s}^{-1} \text{Mpc}^{-1}$ [93–95]. It also agrees with some local measurements including the summary value of [79] $H_0 = 69.25 \pm 2.42 \text{ km s}^{-1} \text{Mpc}^{-1}$ from a joint analysis of $H(z)$, BAO, Pantheon+ SNIa, quasar angular size, reverberation-measured Mg II and C IV quasar, and 118 Amati correlation gamma-ray burst data, and the local $H_0 = 69.03 \pm 1.75 \text{ km s}^{-1} \text{Mpc}^{-1}$ from JWST TRGB+JAGB and SNIa data [96], but is smaller than the local $H_0 = 73.04 \pm 1.04 \text{ km s}^{-1} \text{Mpc}^{-1}$ measured using Cepheids and SNIa data [97], also see [98, 99].

Table VIII lists the current low-redshift, w_0 , and high-redshift, $w(z \rightarrow \infty)$, values of the dynamical dark energy equation of state parameter, $w(z)$, as well as the lensing consistency parameter, A_L , values, measured using P18+lensing+non-CMB data, in a number of dy-

namical dark energy parametrizations. The $\text{XCDM}+A_L$ parametrization value is from [58] and the $w_0w_a\text{CDM}$ ($+A_L$) values are from [19, 50].

In the XCDM parametrization P18+lensing data favor phantom-like ($w < -1$) dynamical dark energy while non-CMB data favor quintessence-like ($w > -1$) behavior, [58], so much so that the cosmological constraints from these two datasets are inconsistent at 3.6σ , thus ruling out the XCDM parametrization at $> 3\sigma$, [58]. Allowing A_L to be an additional free parameter to be determined from data, so now considering the $\text{XCDM}+A_L$ dynamical dark energy parametrization, somewhat reconciles the P18+lensing and the non-CMB constraints, to 2.4σ inconsistency, and a joint P18+lensing+non-CMB data analysis then indicates a 1.3σ preference for a quintessence-like $w_0 = -0.968 \pm 0.024$, but also requires $A_L = 1.101 \pm 0.037$, > 1 at 2.73σ significance, [58]. As noted above, non-CMB data are more effective at constraining $w(z)$ than are P18 or P18+lensing data. In the XCDM parametrization, non-CMB data results in $w_0 = -0.853^{+0.043}_{-0.033}$, while P18+lensing data give $w_0 = -1.55 \pm 0.26$ ($w_0 = -1.34^{+0.26}_{-0.51}$) when $A_L =$

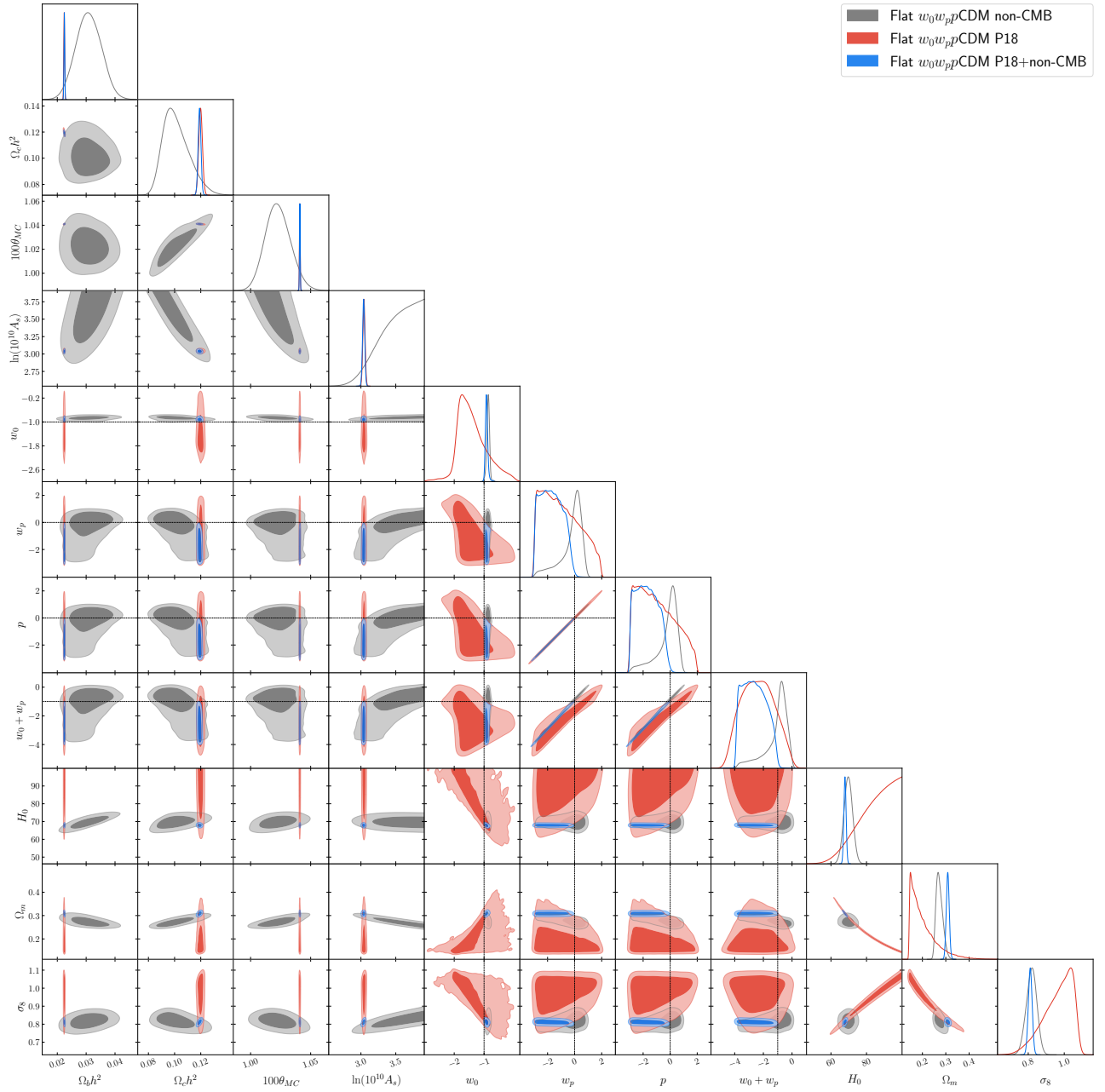


FIG. 7. One-dimensional likelihoods and 1σ and 2σ likelihood confidence contours of flat w_0w_p CDM model parameters favored by non-CMB, P18, and P18+non-CMB datasets. We do not show τ and n_s , which are fixed in the non-CMB data analysis.

1 (when A_L is allowed to vary and determined from P18+lensing data to be 1.054 ± 0.055). This shift in w_0 towards quintessence-like behavior when A_L is allowed to vary away from unity suggests that the observed excess smoothing of some of the Planck CMB multipoles (relative to what is expected in the best-fit Planck cosmological model) is partially responsible for the phantom-like behavior seen in the XCDM parametrization when P18+lensing data are used in the analysis.

When $w(z)$ is parametrized using more than one parameter, such as w_0 and w_a in the w_0w_a CDM

parametrization where $w(z) = w_0 + w_a z / (1 + z)$, there is more freedom so the situation differs a bit from the XCDM case discussed in the previous paragraph. In the two and three parameter $w(z)$ cases we study the P18+lensing constraints and the non-CMB constraints are inconsistent at less than 3σ , even when $A_L = 1$, see Table I and the related discussion above; this differs from what happens in the XCDM case. However, allowing A_L to vary makes the P18+lensing constraints and the non-CMB constraints more consistent, which is similar to what happens in the XCDM case. In the

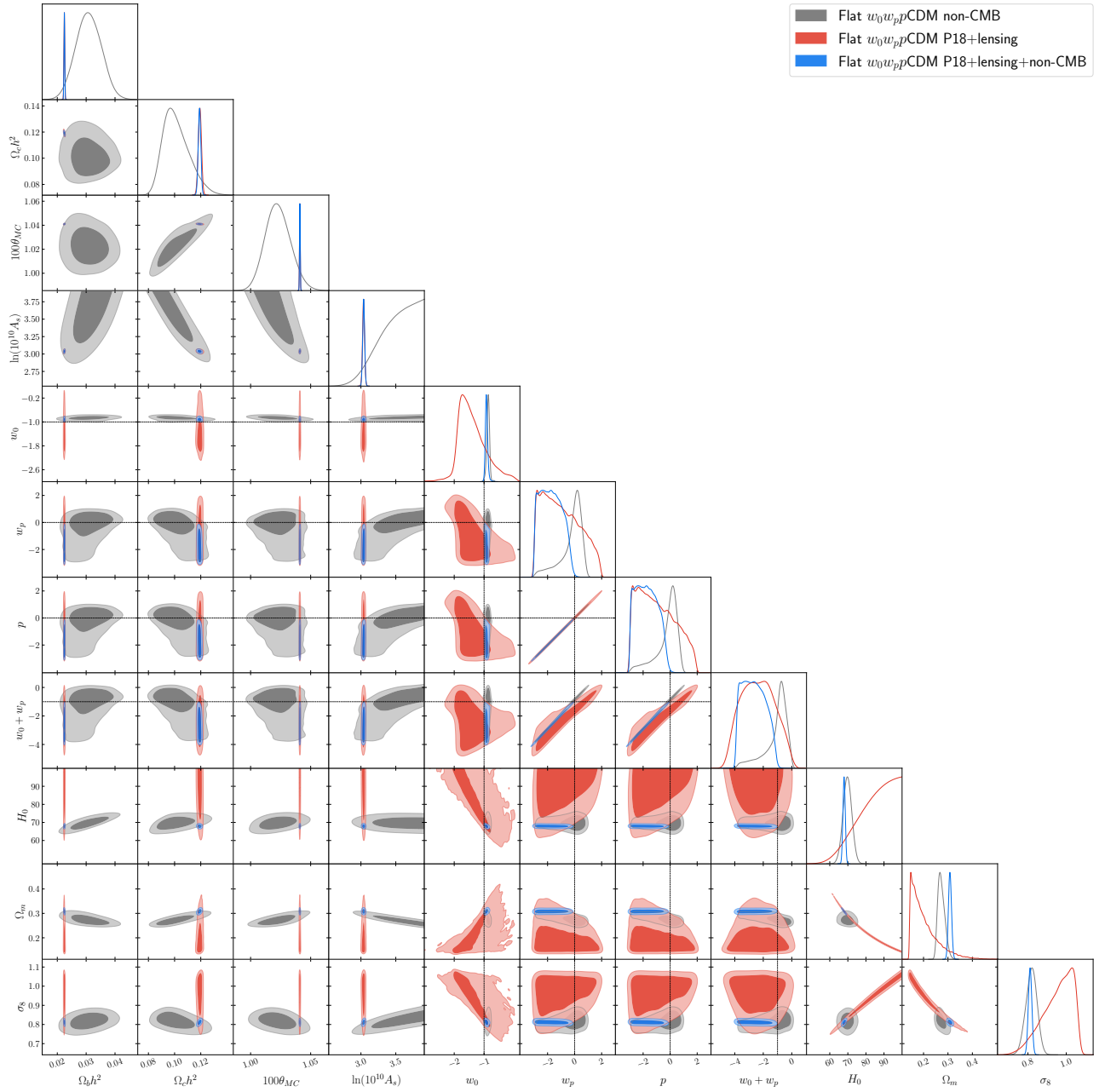


FIG. 8. One-dimensional likelihoods and 1σ and 2σ likelihood confidence contours of flat $w_0 w_p$ CDM model parameters favored by non-CMB, P18+lensing, P18+lensing+non-CMB datasets. We do not show τ and n_s , which are fixed in the non-CMB data analysis.

$w_0 w_a$ CDM case, as discussed in [50], non-CMB data favor quintessence-like behavior, with $w_0 = -0.876 \pm 0.055$, while P18+lensing data favor phantom-like behavior, with $w_0 = -1.24^{+0.44}_{-0.56}$ when $A_L = 1$ and $w_0 = -1.14^{+0.48}_{-0.68}$ with $A_L = 1.046^{+0.038}_{-0.057}$. In this case P18+lensing+non-CMB data favors quintessence-like $w_0 = -0.850 \pm 0.059$ at 2.54σ ($w_0 = -0.879 \pm 0.060$ at 2.02σ) while favoring quintessence-like $w(z \rightarrow \infty) = w_0 + w_a = -1.44^{+0.20}_{-0.17}$ at 2.20σ when $A_L = 1$ ($w(z \rightarrow \infty) = -1.27^{+0.20}_{-0.17}$ at 1.35σ with $A_L = 1.078^{+0.036}_{-0.040}$, > 1 at 1.95σ), see discussion in

[50].

Similar behavior is true for all the other dynamical dark energy parametrizations we study here, as can be seen from the numerical values listed in Table VIII. Excluding Λ CDM, from the results for the other four parametrizations listed in Table VIII, when $A_L = 1$ $w(z \rightarrow \infty)$ is phantom-like at significance ranging from a low of 1.5σ to a high of 2.9σ (with three of the four parametrizations favoring phantom-like behavior at $> 2\sigma$), while when A_L is allowed to vary the support for

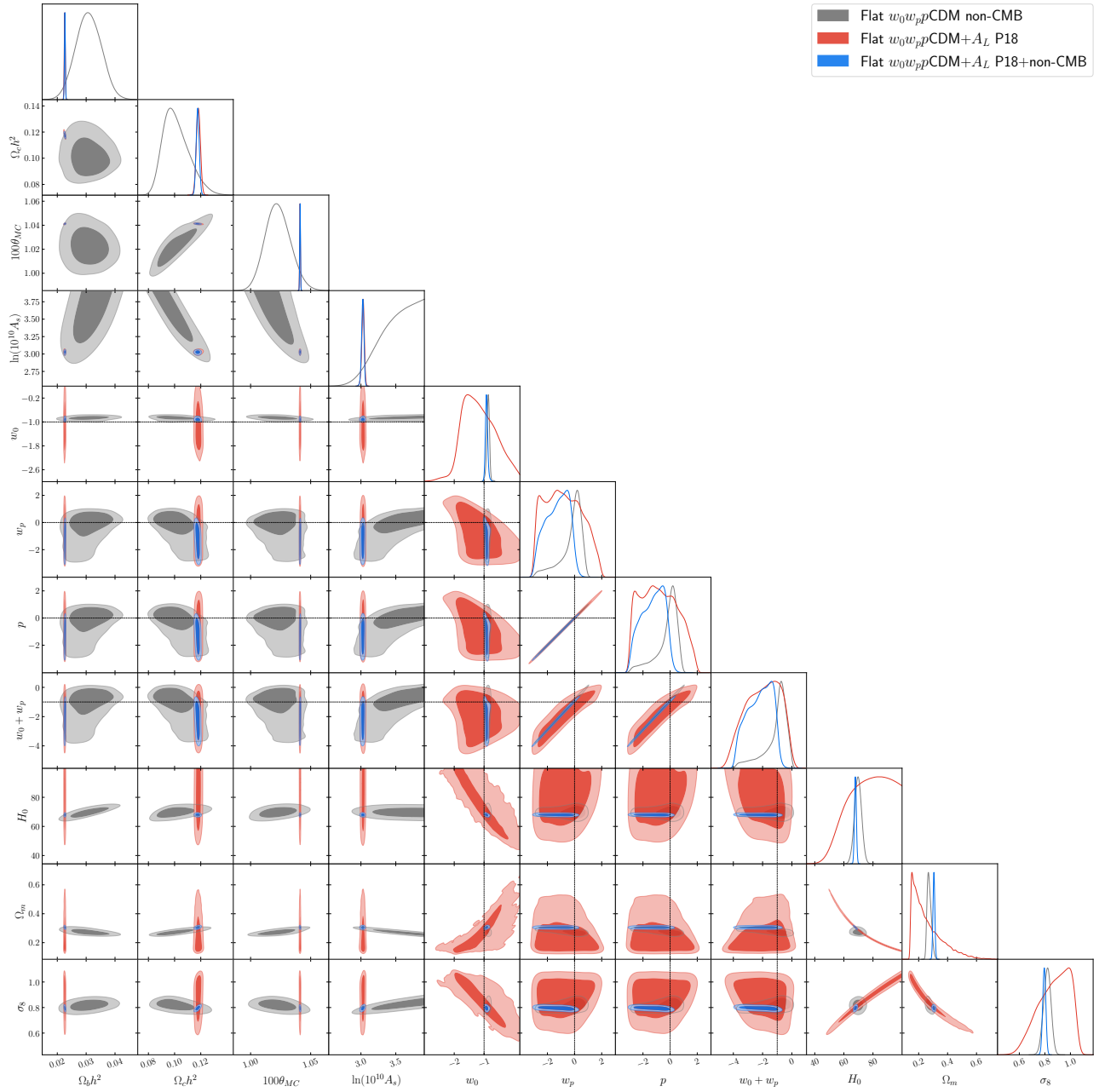


FIG. 9. One-dimensional likelihoods and 1σ and 2σ likelihood confidence contours of flat $w_0w_p p\text{CDM}+A_L$ model parameters favored by non-CMB, P18, and P18+non-CMB datasets. We do not show τ and n_s , which are fixed in the non-CMB data analysis.

phantom-like $w(z \rightarrow \infty)$ has reduced significance ranging from a low of 1.1σ to a high of 1.8σ (with none of the four parametrizations favoring phantom-like behavior at $> 2\sigma$).

We noted above that the two- and three-parameter $w(z)$ parametrizations have more flexibility than the XCDM parametrization and that at low and high redshift the two- and three-parameter parametrizations behave like XCDM parametrizations, but with two different constant w parameters. We also noted above that non-

CMB data is more effective at constraining $w(z)$ since dark energy is not as important at the higher redshift, $z \sim 1100$, where CMB data is more sensitive. In the XCDM parametrization this means that in a joint analysis, like P18+lensing+non-CMB, which is only possible when A_L is allowed to vary (and which brings the P18+lensing constraints and the non-CMB constraints into less than 3σ inconsistency), non-CMB data overwhelms P18+lensing data and results in quintessence-like dynamical dark energy, even though P18+lensing data

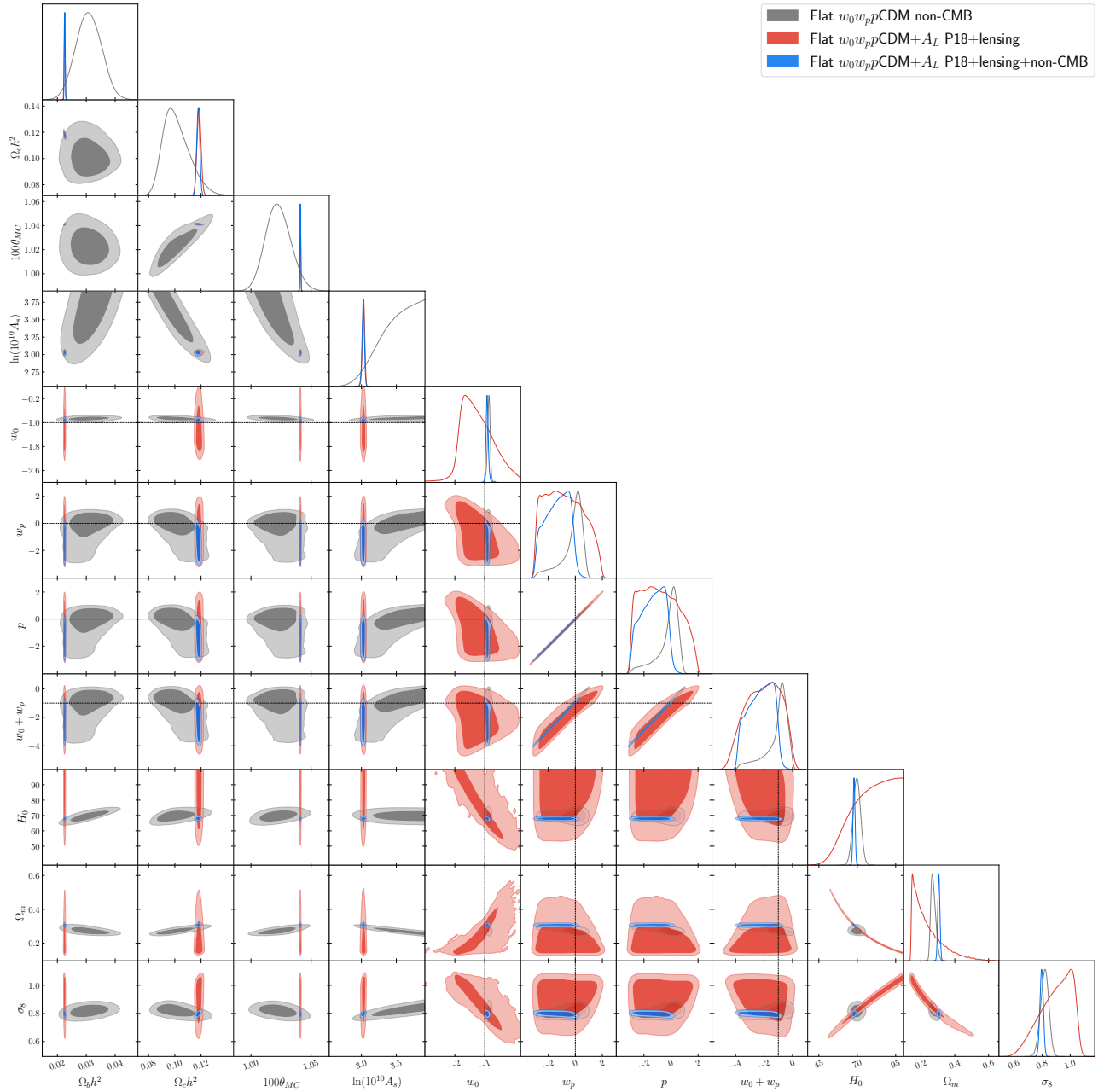


FIG. 10. One-dimensional likelihoods and 1σ and 2σ likelihood confidence contours of flat $w_0 w_p p$ CDM + A_L model parameters favored by non-CMB, P18+lensing, P18+lensing+non-CMB datasets. We do not show τ and n_s , which are fixed in the non-CMB data analysis.

favor phantom-like dynamical dark energy. In the two- and three-parameter $w(z)$ CDM parametrizations, $w(z)$ has more flexibility and while non-CMB data is able to ensure low-redshift w_0 values that are quintessence-like even in joint P18+lensing+non-CMB analyses, and also increase the P18+lensing data high-redshift $w(z \rightarrow \infty)$ values, they are unable to pull it into the more-physical quintessence-like regime, although in all cases they are able to reduce the evidence for phantom-like behavior to below 2σ .

In addition to what is established from the numerical results given in Table I, we can see by comparing the corresponding panels in Figures 5 and 6, 11 and 12, and 17 and 18, that allowing A_L to vary makes the P18 or the P18+lensing cosmological constraints more consistent with the non-CMB ones, compared to the $A_L = 1$ case. In what follows we focus on the P18+lensing data (red contours) and the non-CMB data (gray contours), those shown in the right-hand panels of these figures. In the $w_0 - w_2$ subpanels of the right-hand panels of Fig-

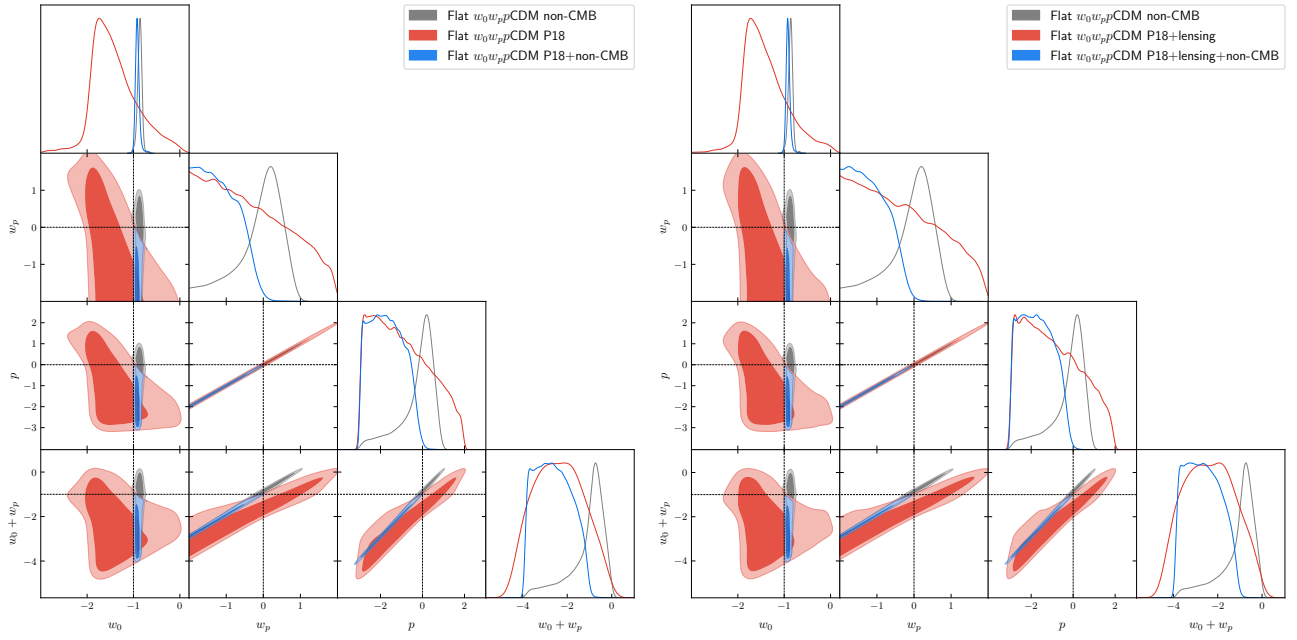


FIG. 11. One-dimensional likelihoods and 1σ and 2σ likelihood confidence contours of w_0 , w_p , p , and $w_0 + w_p$ parameters in the flat w_0w_pp CDM parametrization favored by (left) non-CMB, P18, and P18+non-CMB datasets, and (right) non-CMB, P18+lensing, and P18+lensing+non-CMB datasets.

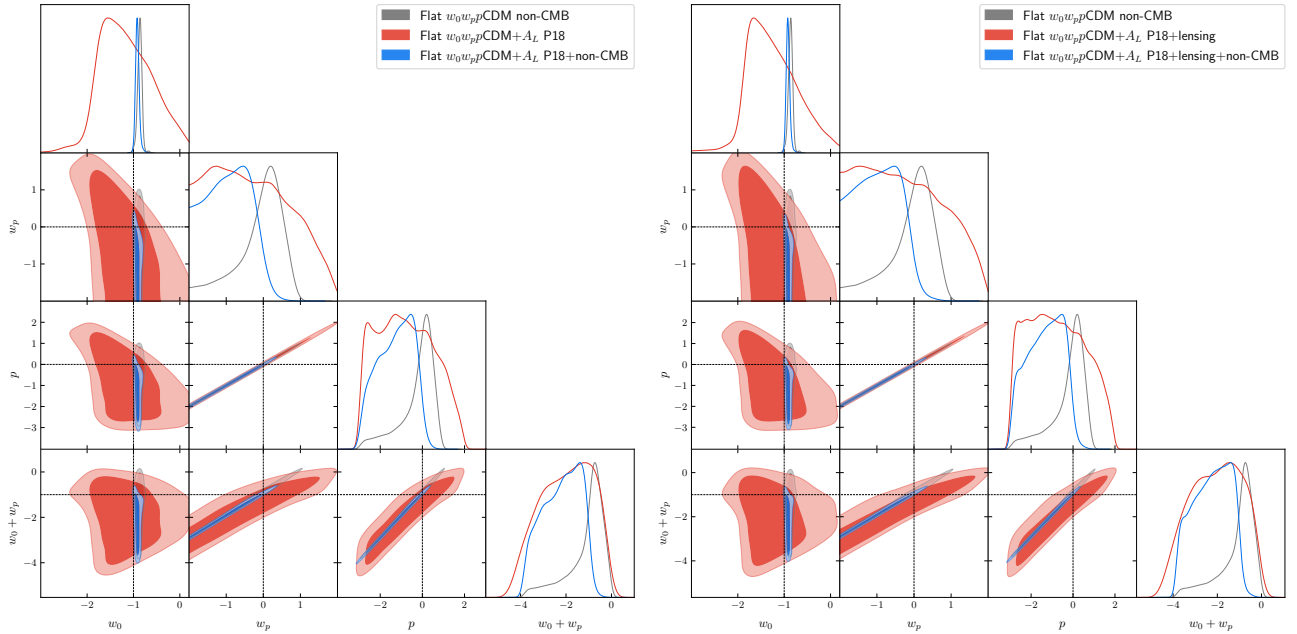


FIG. 12. One-dimensional likelihoods and 1σ and 2σ likelihood confidence contours of w_0 , w_p , p , and $w_0 + w_p$ parameters in the flat w_0w_pp CDM+ A_L model favored by (left) non-CMB, P18, and P18+non-CMB datasets, and (right) non-CMB, P18+lensing, and P18+lensing+non-CMB datasets.

ures 5 and 6, for the w_0w_2 CDM ($+A_L$) parametrizations, one sees when $A_L = 1$ (Fig. 5) the 2σ red and gray contours have some overlap, but when A_L is allowed to vary (Fig. 6) the 2σ grey contours has some overlap with the 1σ red contour and vice versa, with the gray and red

1σ contours almost touching. Similarly, in the $w_0 - w_p$, $w_0 - p$, and $w_p - p$ right-hand subpanels of Figures 11 and 12 for the w_0w_pp CDM ($+A_L$) parametrizations we see a significantly improved consistency between the red and gray contours when going from the $A_L = 1$ case to the

TABLE VI. Mean and 68% (or 95%) confidence limits of flat $w_0w_1w_2$ CDM model parameters from non-CMB, P18, P18+lensing, P18+non-CMB, and P18+lensing+non-CMB data. H_0 has units of $\text{km s}^{-1} \text{Mpc}^{-1}$. We also list the values of χ^2_{\min} , DIC, and AIC and the differences with respect to the values in the flat Λ CDM model for the same dataset, denoted by $\Delta\chi^2_{\min}$, Δ DIC, and Δ AIC, respectively.

Parameter	Non-CMB	P18	P18+lensing	P18+non-CMB	P18+lensing+non-CMB
$\Omega_b h^2$	0.0311 ± 0.0043	0.02240 ± 0.00015	0.02244 ± 0.00015	0.02244 ± 0.00014	0.02245 ± 0.00014
$\Omega_c h^2$	$0.0999^{+0.0064}_{-0.012}$	0.1198 ± 0.0014	0.1192 ± 0.0012	0.1191 ± 0.0011	0.11912 ± 0.00099
$100\theta_{\text{MC}}$	$1.0214^{+0.0092}_{-0.012}$	1.04094 ± 0.00031	1.04101 ± 0.00031	1.04100 ± 0.00030	1.04099 ± 0.00030
τ	0.0540	0.0540 ± 0.0078	0.0520 ± 0.0075	0.0524 ± 0.0077	0.0528 ± 0.0074
n_s	0.9656	0.9656 ± 0.0044	0.9671 ± 0.0042	0.9671 ± 0.0040	0.9670 ± 0.0038
$\ln(10^{10} A_s)$	$3.56 \pm 0.26 (> 3.06)$	3.043 ± 0.016	3.037 ± 0.015	3.038 ± 0.016	3.039 ± 0.014
w_0	$-0.920^{+0.078}_{-0.088}$	$-1.19^{+0.39}_{-0.59}$	$-1.18^{+0.40}_{-0.59}$	$-0.928^{+0.078}_{-0.094}$	$-0.929^{+0.077}_{-0.095}$
w_1	$0.54^{+0.83}_{-0.66}$	$-1.1 \pm 1.3 (< 1.29)$	$-1.1 \pm 1.3 (< 1.36)$	$0.25^{+0.86}_{-0.47}$	$0.27^{+0.87}_{-0.45}$
w_2	$-0.8^{+1.1}_{-1.4}$	$-0.9 \pm 1.4 (< 1.51)$	$-1.1 \pm 1.3 (< 1.54)$	$-1.5 \pm 1.1 (< 0.732)$	$-1.5 \pm 1.1 (< 0.709)$
$w_0 + w_1 + w_2$	$-1.21^{+0.78}_{-0.56}$	$-3.3^{+1.6}_{-1.5}$	$-3.1^{+1.7}_{-1.4}$	$-2.14^{+0.42}_{-0.73}$	$-2.15^{+0.40}_{-0.71}$
H_0	69.8 ± 2.3	$84 \pm 11 (> 63.4)$	$83 \pm 11 (> 63.6)$	67.92 ± 0.64	67.92 ± 0.64
Ω_m	$0.2703^{+0.0093}_{-0.018}$	$0.217^{+0.018}_{-0.074}$	$0.218^{+0.019}_{-0.075}$	0.3084 ± 0.0063	0.3084 ± 0.0063
σ_8	$0.823^{+0.031}_{-0.026}$	$0.950^{+0.12}_{-0.053}$	$0.939^{+0.11}_{-0.052}$	0.812 ± 0.011	0.8118 ± 0.0090
χ^2_{\min}	1457.13	2760.82	2770.51	4232.22	4240.75
$\Delta\chi^2_{\min}$	-12.80	-4.98	-4.20	-8.02	-8.51
DIC	1471.28	2815.65	2824.37	4289.73	4298.65
Δ DIC	-6.83	-2.28	-2.08	-2.60	-2.55
AIC	1471.13	2820.82	2830.51	4292.22	4300.75
Δ AIC	-6.83	+1.02	+1.80	-2.02	-2.51

varying A_L case; there is a degeneracy in the $w_p - p$ subpanels constraint contours that makes it difficult to examine this issue there. This improved consistency is also seen in the $w_0 - w_1$, $w_0 - w_2$, and $w_1 - w_2$ right-hand subpanels of Figures 17 and 18 for the $w_0w_1w_2$ CDM ($+A_L$) parametrizations, most prominently in the $w_0 - w_1$ subpanels.

From the numerical results for the $A_L = 1$ cases in Table VIII, we see that at high- z the dynamical dark energy equation of state parameter $w(z \rightarrow \infty)$ is phantom-like at a significance of 1.52σ (w_0w_p CDM), 2.17σ (w_0w_2 CDM), 2.20σ (w_0w_a CDM), and 2.88σ ($w_0w_1w_2$ CDM) for P18+lensing+non-CMB data. This support for dynamical dark energy over a cosmological constant can also be seen in Figures 5, 11, and 17; for the w_0w_a CDM parametrization see [19]. We focus here on P18+lensing+non-CMB data, and so on the blue contours in the right-hand panels in these figures. In the $w_0 - w_2$ right-hand subpanel in Figure 5 for the w_0w_2 CDM parametrization we see that the Λ CDM model point at $w_0 = -1$ and $w_2 = 0$ lies outside the 2σ blue contour. The same is true for the $w_0 - w_p$, $w_0 - p$, and $w_p - p$ right-hand subpanels of Figure 11 for the

w_0w_p CDM parametrization, where the Λ CDM model corresponds to the point $w_0 = -1$ and $w_p = 0$, $w_0 = -1$ and $p = 0$, and $w_p = 0$ and $p = 0$, respectively, with the Λ CDM model points lying outside the 2σ blue contours in all three subpanels. In the right-hand $w_0 - w_1$, $w_0 - w_2$, and $w_1 - w_2$ subpanels of Figure 17 for the $w_0w_1w_2$ CDM parametrization, the Λ CDM model point $w_0 = -1$, $w_1 = 0$, and $w_2 = 0$ touches the 2σ blue contour in the $w_0 - w_1$ subpanel while lying outside the 2σ blue contours in the $w_0 - w_2$ and $w_1 - w_2$ subpanels.

From the numerical results for the varying A_L cases in Table VIII, we see that at high- z the dynamical dark energy equation of state parameter $w(z \rightarrow \infty)$ is phantom-like at a significance of 1.05σ (w_0w_p CDM+ A_L), 1.35σ (w_0w_a CDM+ A_L), 1.53σ (w_0w_2 CDM+ A_L), and 1.76σ ($w_0w_1w_2$ CDM+ A_L) for P18+lensing+non-CMB data, with $A > 1$ at a significance ranging from 1.83σ to 1.95σ depending on parametrization. This reduced support for dynamical dark energy over a cosmological constant (compared to the corresponding $A_L = 1$ case) can also be seen in Figures 6, 12, and 18; for the w_0w_a CDM+ A_L parametrization see [50]. We again focus on P18+lensing+non-CMB data and so on the blue

TABLE VII. Mean and 68% (or 95%) confidence limits of flat $w_0w_1w_2$ CDM+ A_L model parameters from non-CMB, P18, P18+lensing, P18+non-CMB, and P18+lensing+non-CMB data. H_0 has units of $\text{km s}^{-1} \text{Mpc}^{-1}$. We also list the values of χ^2_{\min} , DIC, and AIC and the differences with respect to the values in the flat Λ CDM model for the same dataset, denoted by $\Delta\chi^2_{\min}$, Δ DIC, and Δ AIC, respectively.

Parameter	Non-CMB	P18	P18+lensing	P18+non-CMB	P18+lensing+non-CMB
$\Omega_b h^2$	0.0311 ± 0.0043	0.02259 ± 0.00017	0.02249 ± 0.00017	0.02263 ± 0.00016	0.02255 ± 0.00015
$\Omega_c h^2$	$0.0999^{+0.0064}_{-0.012}$	0.1181 ± 0.0015	0.1185 ± 0.0015	0.1176 ± 0.0012	0.1178 ± 0.0012
$100\theta_{\text{MC}}$	$1.0214^{+0.0092}_{-0.012}$	1.04115 ± 0.00033	1.04107 ± 0.00033	1.04117 ± 0.00031	1.04113 ± 0.00030
τ	0.0540	$0.0494^{+0.0087}_{-0.0075}$	$0.0491^{+0.0086}_{-0.0074}$	$0.0482^{+0.0085}_{-0.0072}$	$0.0481^{+0.0085}_{-0.0074}$
n_s	0.9656	0.9706 ± 0.0049	0.9688 ± 0.0048	0.9718 ± 0.0043	0.9706 ± 0.0042
$\ln(10^{10} A_s)$	$3.56 \pm 0.26 (> 3.06)$	$3.030^{+0.018}_{-0.016}$	$3.029^{+0.018}_{-0.016}$	$3.026^{+0.017}_{-0.015}$	$3.025^{+0.017}_{-0.015}$
A_L	...	$1.158^{+0.060}_{-0.087}$	$1.040^{+0.041}_{-0.053}$	1.185 ± 0.064	$1.073^{+0.036}_{-0.040}$
w_0	$-0.920^{+0.078}_{-0.088}$	$-0.99^{+0.52}_{-0.67}$	$-1.06^{+0.50}_{-0.66}$	$-0.940^{+0.082}_{-0.10}$	$-0.943^{+0.083}_{-0.095}$
w_1	$0.54^{+0.83}_{-0.66}$	$-0.8 \pm 1.3 (< 1.51)$	$-0.9 \pm 1.4 (< 1.51)$	$0.29^{+0.97}_{-0.54}$	$0.31^{+0.94}_{-0.54}$
w_2	$-0.8^{+1.1}_{-1.4}$	$-0.8 \pm 1.4 (< 1.55)$	$-0.8 \pm 1.4 (< 1.56)$	$-1.2 \pm 1.2 (< 1.18)$	$-1.2 \pm 1.2 (< 1.08)$
$w_0 + w_1 + w_2$	$-1.21^{+0.78}_{-0.56}$	$-2.6^{+1.9}_{-1.1}$	$-2.7^{+1.8}_{-1.3}$	$-1.82^{+0.47}_{-0.82}$	$-1.88^{+0.50}_{-0.79}$
H_0	69.8 ± 2.3	$77^{+20}_{-10} (> 54.9)$	$79 \pm 13 (> 57.6)$	67.96 ± 0.65	67.96 ± 0.64
Ω_m	$0.2703^{+0.0093}_{-0.018}$	$0.267^{+0.036}_{-0.13}$	$0.249^{+0.030}_{-0.11}$	0.3051 ± 0.0064	0.3054 ± 0.0063
σ_8	$0.823^{+0.031}_{-0.026}$	$0.868^{+0.16}_{-0.088}$	$0.891^{+0.14}_{-0.078}$	0.795 ± 0.012	0.797 ± 0.012
χ^2_{\min}	1457.13	2755.91	2770.25	4222.96	4237.21
$\Delta\chi^2_{\min}$	-12.80	-9.89	-4.46	-17.28	-12.05
DIC	1471.28	2813.02	2832.25	4282.32	4296.50
Δ DIC	-6.83	-4.91	-0.17	-10.01	-4.70
AIC	1471.13	2817.91	2832.25	4284.96	4299.21
Δ AIC	-6.83	-1.89	+3.54	-9.28	-4.05

TABLE VIII. Mean and 68% confidence limits of w_0 , $w(z \rightarrow \infty)$, and A_L values in dynamical dark energy parametrizations for P18+lensing+non-CMB data. Significances shown in parentheses for w_0 and $w(z \rightarrow \infty)$ indicate how much larger (smaller) than -1 they are when the following index is qu (ph), while those for A_L indicate how much larger than unity it is. We do not list values for the XCDM parameterization as that is observationally inconsistent at $> 3\sigma$ significance with these data.

Parametrization	w_0	$w(z \rightarrow \infty)$	A_L
XCDM+ A_L	-0.968 ± 0.024 (1.33 σ qu)	-0.968 ± 0.024 (1.33 σ qu)	1.101 ± 0.037 (2.73 σ)
w_0w_a CDM	-0.850 ± 0.059 (2.54 σ qu)	$-1.44^{+0.20}_{-0.17}$ (2.20 σ ph)	1
w_0w_a CDM+ A_L	-0.879 ± 0.060 (2.02 σ qu)	$-1.27^{+0.20}_{-0.17}$ (1.35 σ ph)	$1.078^{+0.036}_{-0.040}$ (1.95 σ)
w_0w_2 CDM	-0.898 ± 0.040 (2.55 σ qu)	$-2.02^{+0.47}_{-0.37}$ (2.17 σ ph)	1
w_0w_2 CDM+ A_L	-0.908 ± 0.040 (2.30 σ qu)	$-1.69^{+0.45}_{-0.36}$ (1.53 σ ph)	1.072 ± 0.038 (1.89 σ)
w_0w_p CDM	$-0.916^{+0.031}_{-0.045}$ (1.87 σ qu)	$-1.73^{+0.48}_{-1.2}$ (1.52 σ ph)	1
w_0w_p CDM+ A_L	$-0.917^{+0.032}_{-0.042}$ (1.98 σ qu)	$-2.26^{+1.2}_{-0.63}$ (1.05 σ ph)	1.072 ± 0.038 (1.89 σ)
$w_0w_1w_2$ CDM	$-0.929^{+0.077}_{-0.095}$ (0.747 σ qu)	$-2.15^{+0.40}_{-0.71}$ (2.88 σ ph)	1
$w_0w_1w_2$ CDM+ A_L	$-0.943^{+0.083}_{-0.095}$ (0.600 σ qu)	$-1.88^{+0.50}_{-0.79}$ (1.76 σ ph)	$1.073^{+0.036}_{-0.040}$ (1.83 σ)

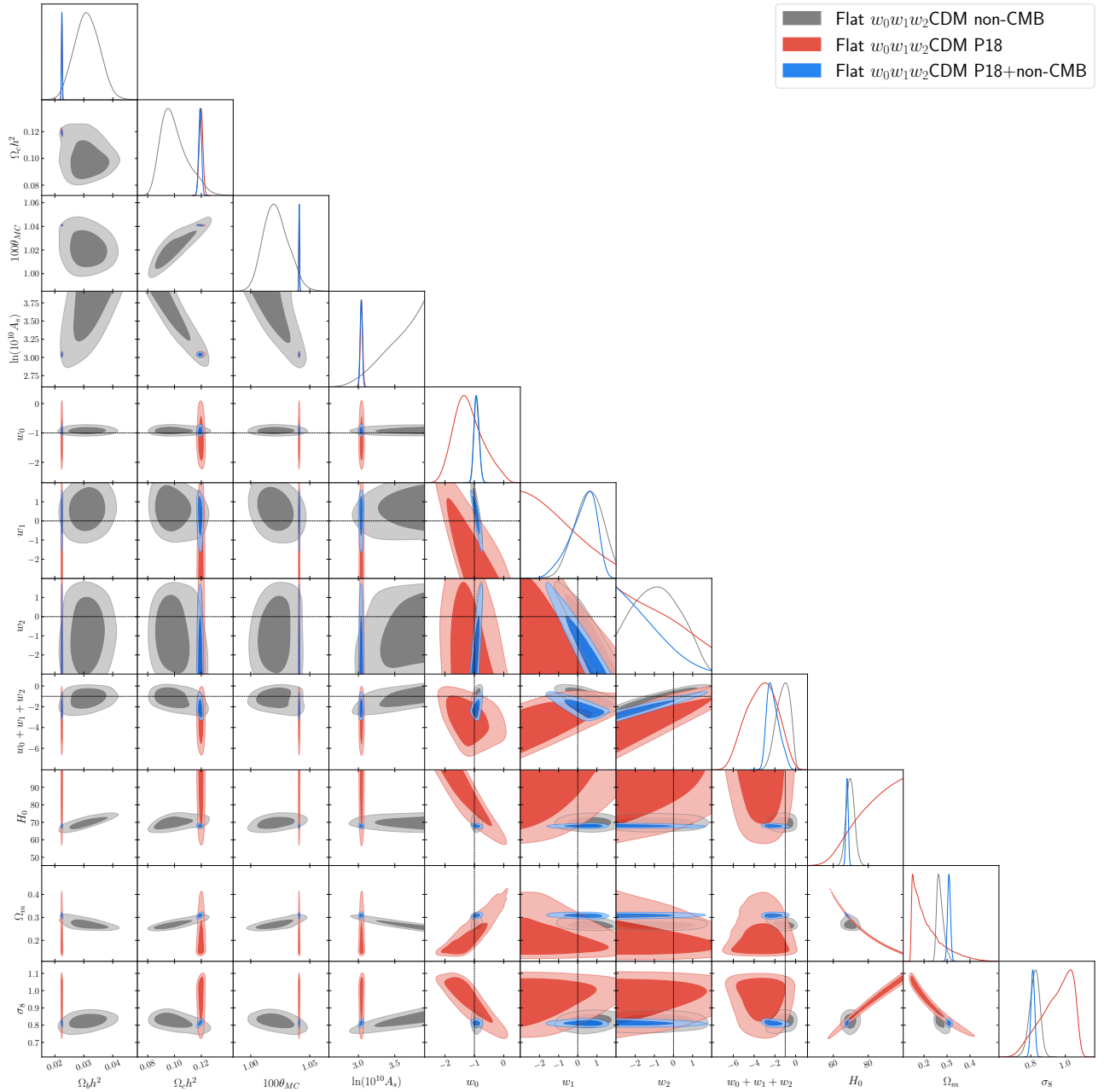


FIG. 13. One-dimensional likelihoods and 1σ and 2σ likelihood confidence contours of flat $w_0w_1w_2$ CDM model parameters favored by non-CMB, P18, and P18+non-CMB datasets. We do not show τ and n_s , which are fixed in the non-CMB data analysis.

contours in the right-hand panels in these figures. In the $w_0 - w_2$ right-hand subpanel in Figure 6 for the w_0w_2 CDM+ A_L parametrization we see that the Λ CDM model point at $w_0 = -1$ and $w_2 = 0$ lies between the 1σ and 2σ blue contours. The same is true for the $w_0 - w_p$, $w_0 - p$, and $w_p - p$ right-hand subpanels of Figure 12 for the w_0w_p pCDM+ A_L parametrization, where the Λ CDM model corresponds to the point $w_0 = -1$ and $w_p = 0$, $w_0 = -1$ and $p = 0$, and $w_p = 0$ and $p = 0$, respectively, with the Λ CDM model points ly-

ing between the 1σ and 2σ blue contours, but closer to the 1σ ones, in all three subpanels. In the right-hand $w_0 - w_1$, $w_0 - w_2$, and $w_1 - w_2$ subpanels of Figure 18 for the $w_0w_1w_2$ CDM+ A_L parametrization, the Λ CDM model point $w_0 = -1$, $w_1 = 0$, and $w_2 = 0$ touches the 2σ blue contours in the $w_0 - w_1$ and $w_0 - w_2$ subpanels while lying between the 1σ and 2σ blue contours in the $w_1 - w_2$ subpanel.

In summary, unlike in the flat Λ CDM (+ A_L) models, tables IV and VII in [58], in the dynamical dark

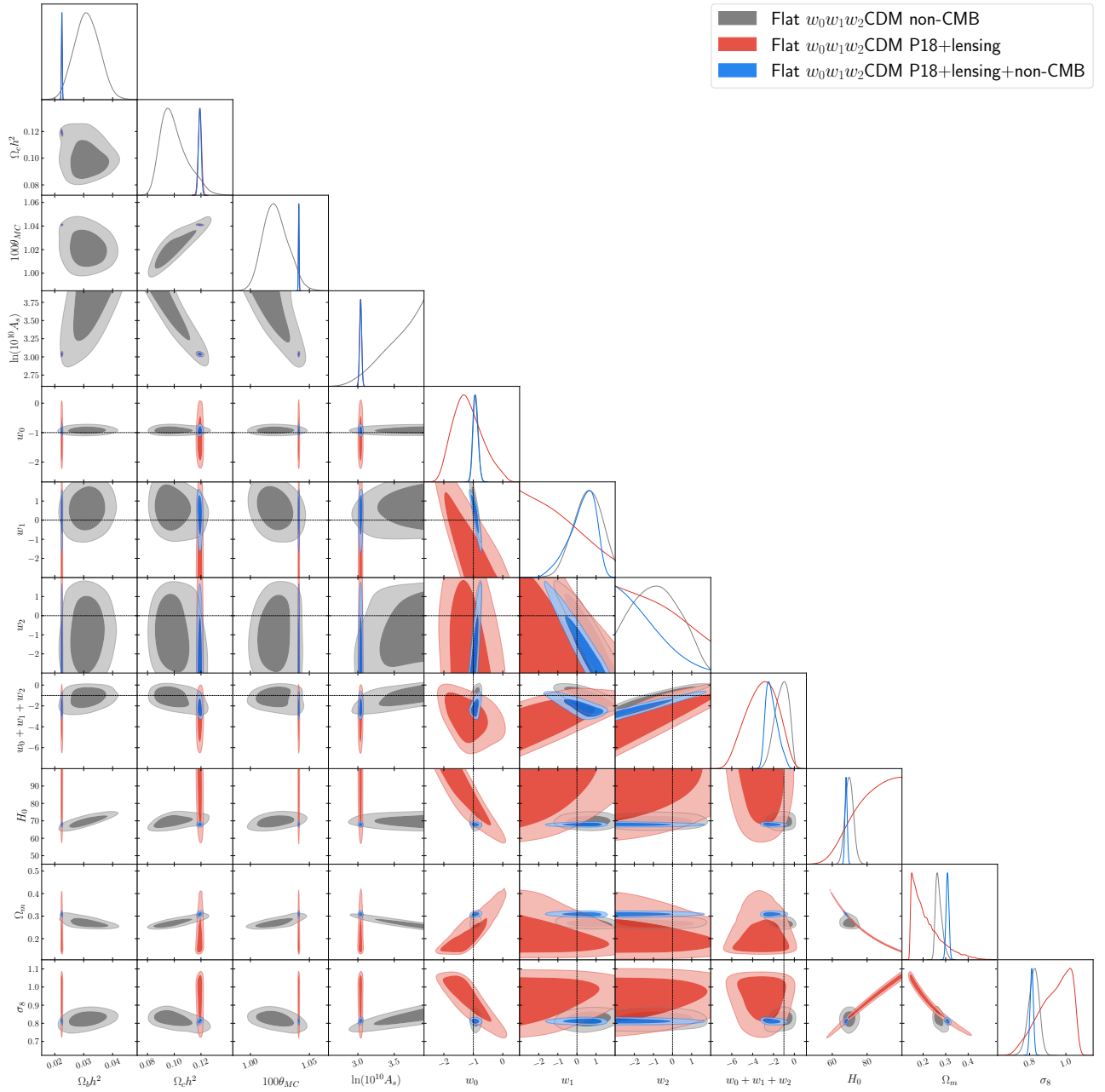


FIG. 14. One-dimensional likelihoods and 1σ and 2σ likelihood confidence contours of flat $w_0w_1w_2$ CDM model parameters favored by non-CMB, P18+lensing, P18+lensing+non-CMB datasets. We do not show τ and n_s , which are fixed in the non-CMB data analysis.

energy parametrizations we consider, including the flat Λ CDM+ A_L parametrization, table XI of [58], and the flat w_0w_a CDM (+ A_L) parametrizations, [19, 50], and the flat w_0w_2 CDM (+ A_L), w_0w_p CDM (+ A_L), and $w_0w_1w_2$ CDM (+ A_L) parametrizations, Tables II–VII, high- z P18 and P18+lensing data favor phantom-like dynamical dark energy, higher H_0 values, and smaller Ω_m values, all with larger error bars, while low- z non-CMB data favor quintessence-like dynamical dark energy, lower H_0 values, and larger Ω_m values, all with smaller er-

ror bars. Joint analysis of P18+lensing+non-CMB data breaks the parameter degeneracy and compromises by picking a slightly lower H_0 value and a slightly larger Ω_m value than are favored by non-CMB data but with much more restrictive error bars. Excluding the Λ CDM+ A_L case, in the two- and three-parameter $w(z)$ CDM cases the joint P18+lensing+non-CMB analysis results in a less, but still, phantom-like $w(z \rightarrow \infty) < -1$ when $A_L = 1$, which becomes even less, but still, phantom-like when A_L is allowed to vary and be simultaneously determined from

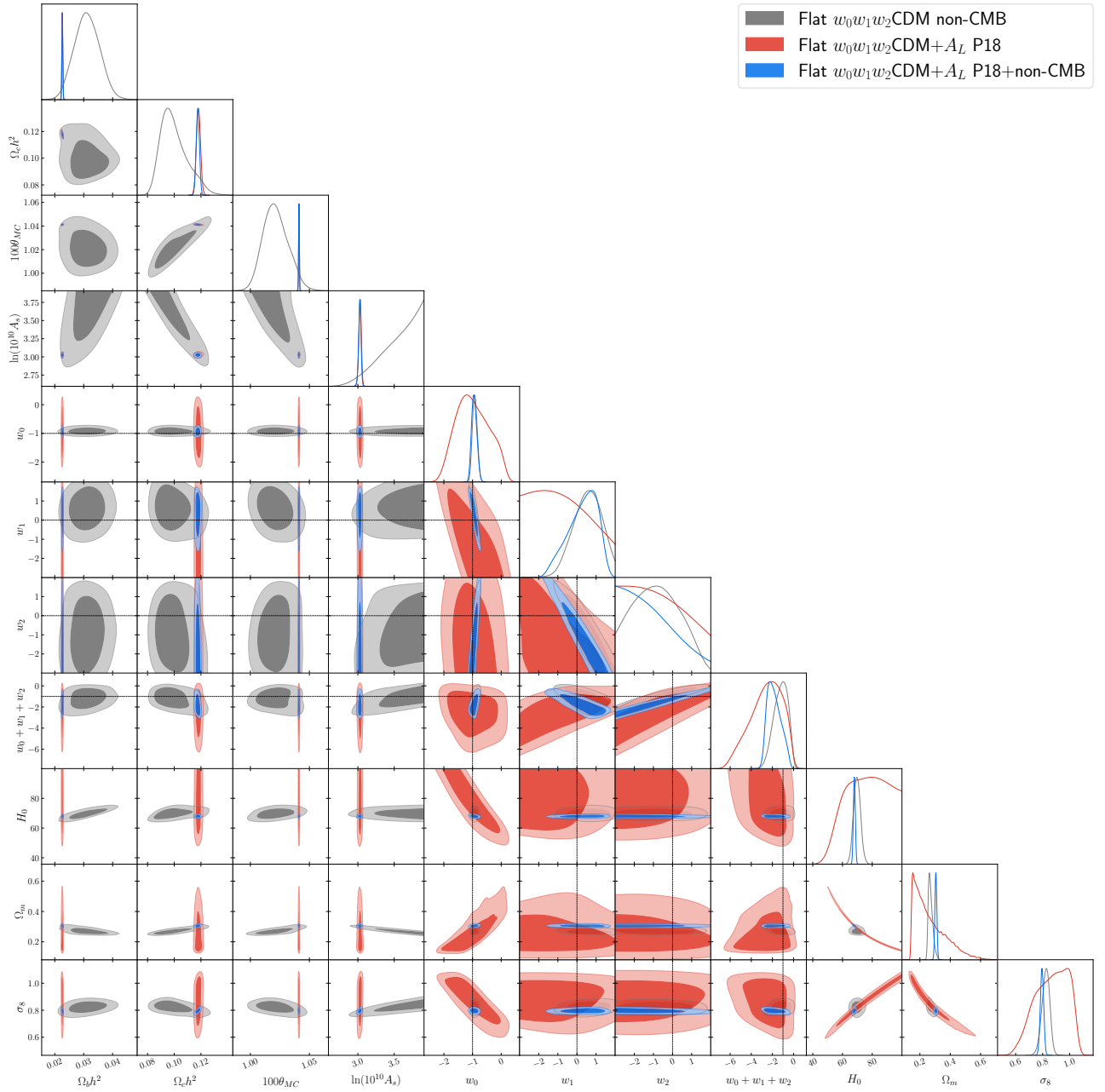


FIG. 15. One-dimensional likelihoods and 1σ and 2σ likelihood confidence contours of flat $w_0 w_1 w_2 \text{CDM} + A_L$ model parameters favored by non-CMB, P18, and P18+non-CMB datasets. We do not show τ and n_s , which are fixed in the non-CMB data analysis.

these data. This evidence for phantom-like dark energy in these parametrizations is neither due to DESI BAO data (which we do not use), nor is it due to Pantheon+ or other SNIa data (see [19, 50] for analysis and discussion in the $w_0 w_a \text{CDM}$ case). Because all the parametrizations we study reduce to the ΛCDM parametrization at high z , all the parametrizations favor phantom-like dynamical dark energy at larger z . When $A_L = 1$ they favor phantom-like behavior at a significance of $\gtrsim 2\sigma$, while when A_L varies the significance drops to $\gtrsim 1\sigma$. This

suggest that a significant part of the evidence for higher- z phantom-like behavior in these parametrizations is a consequence of the excess smoothing (relative to what is expected in the best-fit cosmological model) observed in some of the Planck CMB anisotropy multipoles.

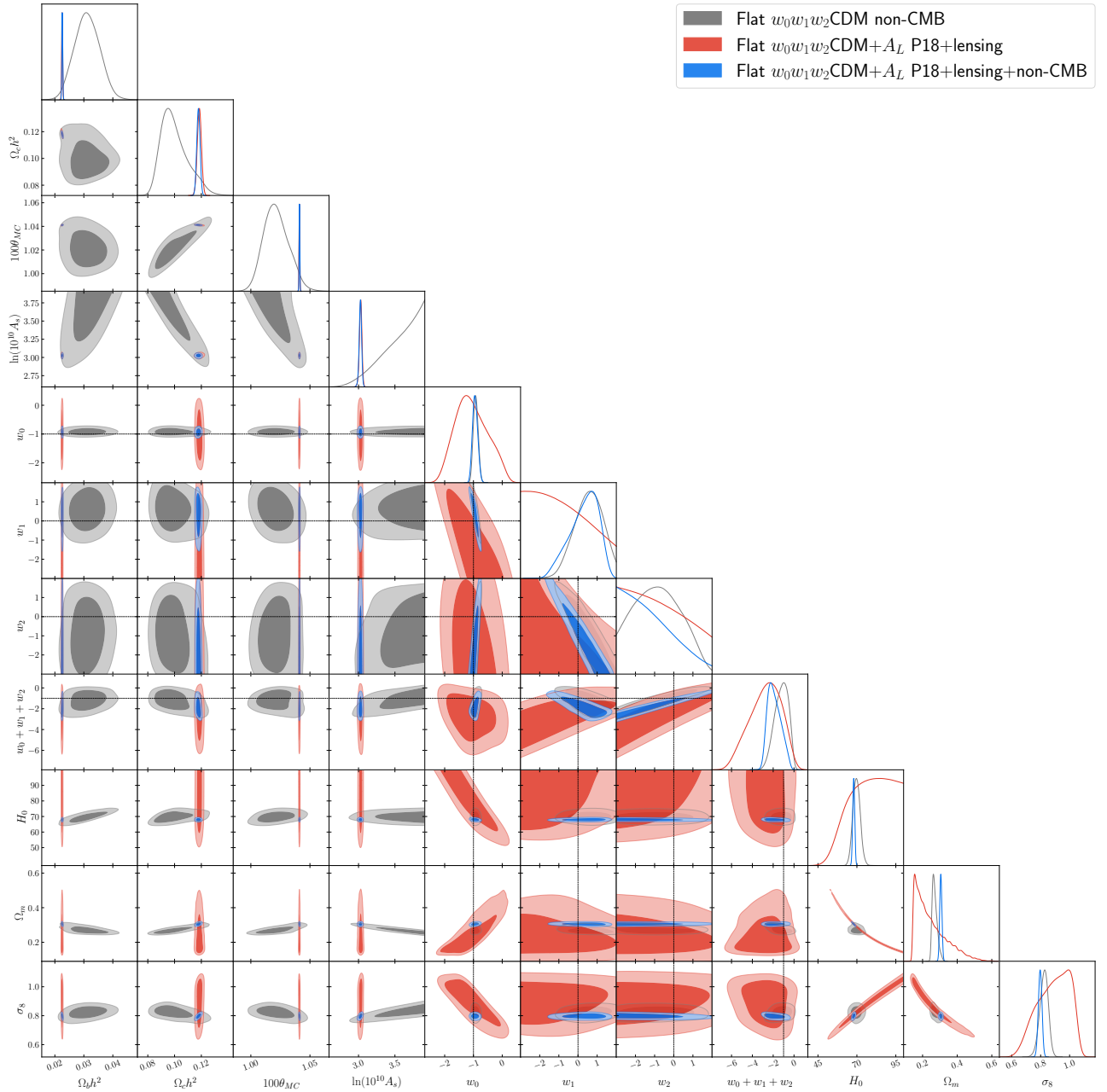


FIG. 16. One-dimensional likelihoods and 1σ and 2σ likelihood confidence contours of flat $w_0w_1w_2\text{CDM}+A_L$ model parameters favored by non-CMB, P18+lensing, P18+lensing+non-CMB datasets. We do not show τ and n_s , which are fixed in the non-CMB data analysis.

V. CONCLUSION

Adding to the results of [19, 50], here we analyze three new $w(z)\text{CDM} (+A_L)$ dynamical dark energy parametrizations. From where the ΛCDM model point lies relative to the P18+lensing+non-CMB data cosmological parameter constraint contours of the four $w(z)\text{CDM} (+A_L)$ parametrizations, we find that dark energy dynamics is favored over a cosmological constant by $\gtrsim 2\sigma$ when $A_L = 1$, but only by $\gtrsim 1\sigma$ when A_L is

allowed to vary (and is simultaneously determined from these data to be > 1 at $\sim 2\sigma$ significance). The non-CMB data compilation we use is the largest such compilation of independent, mutually-consistent non-CMB data [58]. It is the dominant part of the P18+lensing+non-CMB compilation at low z when these data favor quintessence-like dark energy dynamics. At high z , when P18+lensing data are dominant, these data favor phantom-like dark energy dynamics, at significance ranging from 1.5σ to 2.9σ when $A_L = 1$ and at a reduced significance ranging

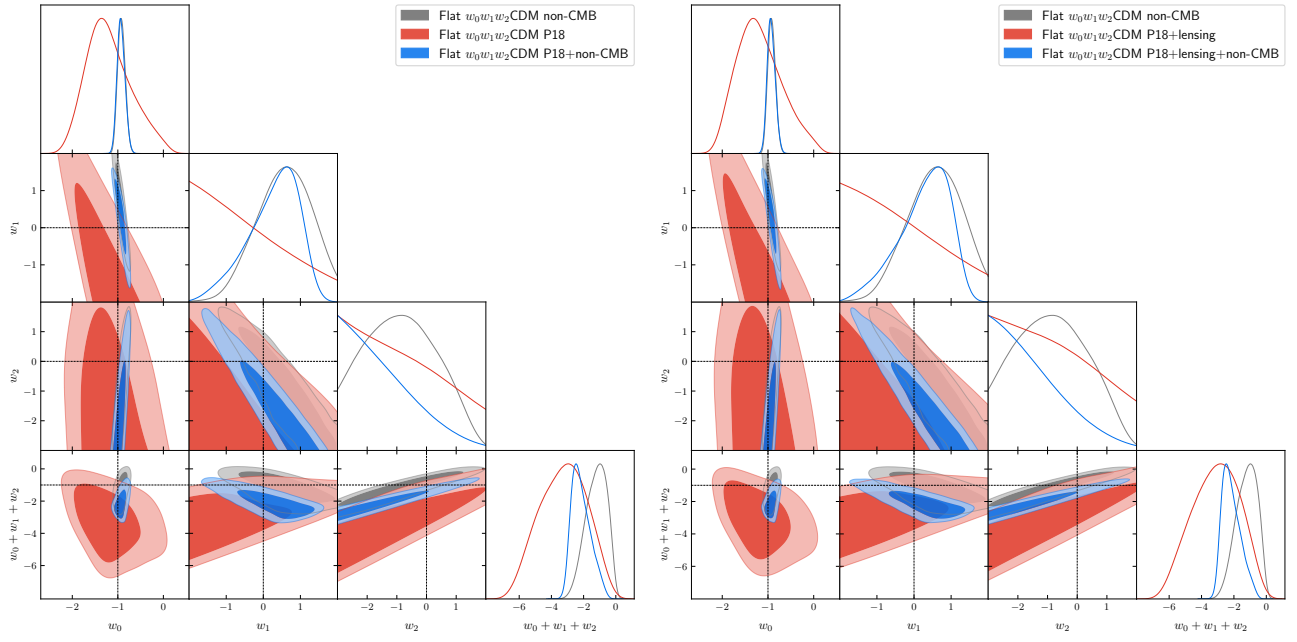


FIG. 17. One-dimensional likelihoods and 1σ and 2σ likelihood confidence contours of w_0 , w_1 , w_2 , and $w_0 + w_1 + w_2$ parameters in the flat $w_0w_1w_2$ CDM parametrization favored by (left) non-CMB, P18, and P18+non-CMB datasets, and (right) non-CMB, P18+lensing, and P18+lensing+non-CMB datasets.

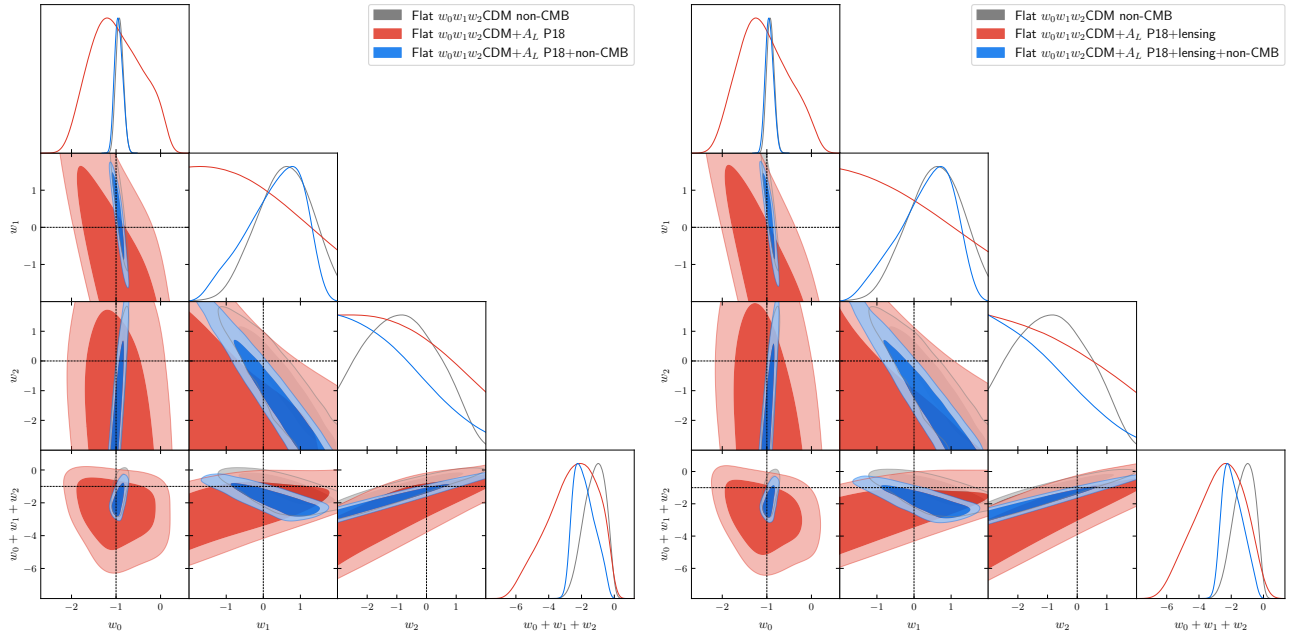


FIG. 18. One-dimensional likelihoods and 1σ and 2σ likelihood confidence contours of w_0 , w_1 , w_2 , and $w_0 + w_1 + w_2$ parameters in the flat $w_0w_1w_2$ CDM+ A_L parametrization favored by (left) non-CMB, P18, and P18+non-CMB datasets, and (right) non-CMB, P18+lensing, and P18+lensing+non-CMB datasets.

from 1.1σ to 1.8σ when A_L is allowed to vary and be simultaneously determined from these data.

From ΔDIC values relative to the Λ CDM model, we find the $w(z)$ CDM parametrizations are *positively* favored over the Λ CDM model, for both the $A_L = 1$

(with ΔDIC values ranging from -2.45 to -3.98) and the varying A_L (with ΔDIC values ranging from -4.37 to -5.60) cases, with the varying A_L case *weakly to positively* favored over the $A_L = 1$ case (with relative ΔDIC values ranging from -1.62 to -2.15), because allowing

A_L to vary results in better reconciliation of the P18 or P18+lensing data constraints and the non-CMB data constraints.

This evidence for dark energy dynamics in the $w(z)$ CDM parametrizations does not depend on the use of DESI data, which we have not used here, also see [19, 50]. Nor does it depend on the use of Pantheon+SNIa (or any SNIa data), see [19] for a detailed study of this in the w_0w_a CDM parametrization. The shifts toward quintessence-like behavior of the measured $w(z)$'s, in the $w(z)$ CDM ($+A_L$) parametrizations, when A_L is allowed to vary compared to the corresponding $A_L = 1$ case, suggest that this evidence for dark energy dynamics at least partially depends on the observed excess smoothing of some of the Planck CMB anisotropy multipoles, also see [50]. In this context, it is interesting that from the new PR4 Planck data release [100], in the flat Λ CDM+ A_L model, where A_L is allowed to vary, PR4

data including lensing data give $A_L = 1.037 \pm 0.37$, favoring $A_L > 1$ at 1σ , which is smaller than the 1.78σ significance for $A_L > 1$ that follows from the P18+lensing data result $A_L = 1.073 \pm 0.041$.

While our results are interesting, they are not based on a physically consistent dynamical dark energy model, e.g., ϕ CDM, [101, 102]; they are based on $w(z)$ CDM parametrizations that reduce to different XCDM parametrizations at low and high z . Our results are also not that statistically significant. However, they highlight a number of interesting issues that deserve additional scrutiny.

ACKNOWLEDGMENTS

C.-G.P. was supported by a National Research Foundation of Korea (NRF) grant funded by the Korea government (MSIT) No. RS-2023-00246367.

-
- [1] P. J. E. Peebles, Tests of Cosmological Models Constrained by Inflation, *Astrophys. J.* **284**, 439 (1984).
- [2] L. Perivolaropoulos and F. Skara, Challenges for Λ CDM: An update, *New Astron. Rev.* **95**, 101659 (2022), arXiv:2105.05208 [astro-ph.CO].
- [3] M. Moresco *et al.*, Unveiling the Universe with emerging cosmological probes, *Living Rev. Rel.* **25**, 6 (2022), arXiv:2201.07241 [astro-ph.CO].
- [4] E. Abdalla *et al.*, Cosmology intertwined: A review of the particle physics, astrophysics, and cosmology associated with the cosmological tensions and anomalies, *JHEAp* **34**, 49 (2022), arXiv:2203.06142 [astro-ph.CO].
- [5] J.-P. Hu and F.-Y. Wang, Hubble Tension: The Evidence of New Physics, *Universe* **9**, 94 (2023), arXiv:2302.05709 [astro-ph.CO].
- [6] A. G. Adame *et al.* (DESI), DESI 2024 VI: Cosmological Constraints from the Measurements of Baryon Acoustic Oscillations, (2024), arXiv:2404.03002 [astro-ph.CO].
- [7] M. Chevallier and D. Polarski, Accelerating universes with scaling dark matter, *Int. J. Mod. Phys. D* **10**, 213 (2001), arXiv:gr-qc/0009008.
- [8] E. V. Linder, Exploring the expansion history of the universe, *Phys. Rev. Lett.* **90**, 091301 (2003), arXiv:astro-ph/0208512.
- [9] Y. Tada and T. Terada, Quintessential interpretation of the evolving dark energy in light of DESI observations, *Phys. Rev. D* **109**, L121305 (2024), arXiv:2404.05722 [astro-ph.CO].
- [10] W. Yin, Cosmic clues: DESI, dark energy, and the cosmological constant problem, *JHEP* **05**, 327, arXiv:2404.06444 [hep-ph].
- [11] D. Wang, Constraining Cosmological Physics with DESI BAO Observations, (2024), arXiv:2404.06796 [astro-ph.CO].
- [12] O. Luongo and M. Muccino, Model-independent cosmographic constraints from DESI 2024, *Astron. Astrophys.* **690**, A40 (2024), arXiv:2404.07070 [astro-ph.CO].
- [13] M. Cortês and A. R. Liddle, Interpreting DESI's evidence for evolving dark energy, *JCAP* **12**, 007, arXiv:2404.08056 [astro-ph.CO].
- [14] E. O. Colgáin, M. G. Dainotti, S. Capozziello, S. Pourojaghi, M. M. Sheikh-Jabbari, and D. Stojkovic, Does DESI 2024 Confirm Λ CDM?, (2024), arXiv:2404.08633 [astro-ph.CO].
- [15] D. Wang, The Self-Consistency of DESI Analysis and Comment on "Does DESI 2024 Confirm Λ CDM?", (2024), arXiv:2404.13833 [astro-ph.CO].
- [16] K. V. Berghaus, J. A. Kable, and V. Miranda, Quantifying scalar field dynamics with DESI 2024 Y1 BAO measurements, *Phys. Rev. D* **110**, 103524 (2024), arXiv:2404.14341 [astro-ph.CO].
- [17] H. Wang and Y.-S. Piao, Dark energy in light of recent DESI BAO and Hubble tension, (2024), arXiv:2404.18579 [astro-ph.CO].
- [18] Y. Yang, X. Ren, Q. Wang, Z. Lu, D. Zhang, Y.-F. Cai, and E. N. Saridakis, Quintom cosmology and modified gravity after DESI 2024, *Sci. Bull.* **69**, 2698 (2024), arXiv:2404.19437 [astro-ph.CO].
- [19] C.-G. Park, J. de Cruz Pérez, and B. Ratra, Using non-DESI data to confirm and strengthen the DESI 2024 spatially flat w_0w_a CDM cosmological parametrization result, *Phys. Rev. D* **110**, 123533 (2024), arXiv:2405.00502 [astro-ph.CO].
- [20] D. Shlivko and P. J. Steinhardt, Assessing observational constraints on dark energy, *Phys. Lett. B* **855**, 138826 (2024), arXiv:2405.03933 [astro-ph.CO].
- [21] Z. Huang *et al.*, Key drivers of the preference for dynamic dark energy, *Phys. Rev. D* **110**, 123512 (2024), arXiv:2405.03983 [astro-ph.CO].
- [22] R. Calderon *et al.* (DESI), DESI 2024: reconstructing dark energy using crossing statistics with DESI DR1 BAO data, *JCAP* **10**, 048, arXiv:2405.04216 [astro-ph.CO].
- [23] B. R. Dinda, A new diagnostic for the null test of dynamical dark energy in light of DESI 2024 and other BAO data, *JCAP* **09**, 062, arXiv:2405.06618 [astro-ph.CO].

- [24] D. Andriot, S. Parameswaran, D. Tsimpis, T. Wrase, and I. Zavala, Exponential quintessence: curved, steep and stringy?, *JHEP* **08**, 117, arXiv:2405.09323 [hep-th].
- [25] K. Lodha *et al.* (DESI), DESI 2024: Constraints on Physics-Focused Aspects of Dark Energy using DESI DR1 BAO Data, (2024), arXiv:2405.13588 [astro-ph.CO].
- [26] S. Bhattacharya, G. Borghetto, A. Malhotra, S. Parameswaran, G. Tasinato, and I. Zavala, Cosmological constraints on curved quintessence, *JCAP* **09**, 073, arXiv:2405.17396 [astro-ph.CO].
- [27] O. F. Ramadan, J. Sakstein, and D. Rubin, DESI constraints on exponential quintessence, *Phys. Rev. D* **110**, L041303 (2024), arXiv:2405.18747 [astro-ph.CO].
- [28] P. Mukherjee and A. A. Sen, Model-independent cosmological inference post DESI DR1 BAO measurements, *Phys. Rev. D* **110**, 123502 (2024), arXiv:2405.19178 [astro-ph.CO].
- [29] N. Roy, Dynamical dark energy in the light of DESI 2024 data, (2024), arXiv:2406.00634 [astro-ph.CO].
- [30] H. Wang, Z.-Y. Peng, and Y.-S. Piao, Can recent DESI BAO measurements accommodate a negative cosmological constant?, (2024), arXiv:2406.03395 [astro-ph.CO].
- [31] J. J. Heckman, O. F. Ramadan, and J. Sakstein, First Constraints on a Pixelated Universe in Light of DESI, (2024), arXiv:2406.04408 [astro-ph.CO].
- [32] I. D. Gialamas, G. Hütsi, K. Kannike, A. Racioppi, M. Raidal, M. Vasar, and H. Veermäe, Interpreting DESI 2024 BAO: late-time dynamical dark energy or a local effect?, (2024), arXiv:2406.07533 [astro-ph.CO].
- [33] A. Notari, M. Redi, and A. Tesi, Consistent theories for the DESI dark energy fit, *JCAP* **11**, 025, arXiv:2406.08459 [astro-ph.CO].
- [34] G. Liu, Y. Wang, and W. Zhao, Impact of LRG1 and LRG2 in DESI 2024 BAO data on dark energy evolution, (2024), arXiv:2407.04385 [astro-ph.CO].
- [35] L. Orchard and V. H. Cárdenas, Probing dark energy evolution post-DESI 2024, *Phys. Dark Univ.* **46**, 101678 (2024), arXiv:2407.05579 [astro-ph.CO].
- [36] V. Patel, A. Chakraborty, and L. Amendola, The prior dependence of the DESI results, (2024), arXiv:2407.06586 [astro-ph.CO].
- [37] H. Wang, G. Ye, and Y.-S. Piao, Impact of evolving dark energy on the search for primordial gravitational waves, (2024), arXiv:2407.11263 [astro-ph.CO].
- [38] T.-N. Li, P.-J. Wu, G.-H. Du, S.-J. Jin, H.-L. Li, J.-F. Zhang, and X. Zhang, Constraints on Interacting Dark Energy Models from the DESI Baryon Acoustic Oscillation and DES Supernovae Data, *Astrophys. J.* **976**, 1 (2024), arXiv:2407.14934 [astro-ph.CO].
- [39] W. Giarè, M. Najafi, S. Pan, E. Di Valentino, and J. T. Firouzjaee, Robust preference for Dynamical Dark Energy in DESI BAO and SN measurements, *JCAP* **10**, 035, arXiv:2407.16689 [astro-ph.CO].
- [40] B. R. Dinda and R. Maartens, Model-agnostic assessment of dark energy after DESI DR1 BAO, (2024), arXiv:2407.17252 [astro-ph.CO].
- [41] J.-Q. Jiang, W. Giarè, S. Gariazzo, M. G. Dainotti, E. Di Valentino, O. Mena, D. Pedrotti, S. S. da Costa, and S. Vagnozzi, Neutrino cosmology after DESI: tightest mass upper limits, preference for the normal ordering, and tension with terrestrial observations, (2024), arXiv:2407.18047 [astro-ph.CO].
- [42] J.-Q. Jiang, D. Pedrotti, S. S. da Costa, and S. Vagnozzi, Nonparametric late-time expansion history reconstruction and implications for the Hubble tension in light of recent DESI and type Ia supernovae data, *Phys. Rev. D* **110**, 123519 (2024), arXiv:2408.02365 [astro-ph.CO].
- [43] A. C. Alfano, O. Luongo, and M. Muccino, Cosmological constraints from calibrated Ep - E_{iso} gamma-ray burst correlation by using DESI 2024 data release, *JCAP* **12**, 055, arXiv:2408.02536 [astro-ph.CO].
- [44] B. Ghosh and C. Bengaly, Consistency tests between SDSS and DESI BAO measurements, *Phys. Dark Univ.* **46**, 101699 (2024), arXiv:2408.04432 [astro-ph.CO].
- [45] S. Pourojaghi, M. Malekjani, and Z. Davari, Λ CDM model against cosmography: A possible deviation after DESI 2024, (2024), arXiv:2408.10704 [astro-ph.CO].
- [46] J. a. Rebouças, D. H. F. de Souza, K. Zhong, V. Miranda, and R. Rosenfeld, Investigating Late-Time Dark Energy and Massive Neutrinos in Light of DESI Y1 BAO, (2024), arXiv:2408.14628 [astro-ph.CO].
- [47] W. J. Wolf, C. García-García, D. J. Bartlett, and P. G. Ferreira, Scant evidence for thawing quintessence, *Phys. Rev. D* **110**, 083528 (2024), arXiv:2408.17318 [astro-ph.CO].
- [48] S. Roy Choudhury and T. Okumura, Updated Cosmological Constraints in Extended Parameter Space with Planck PR4, DESI Baryon Acoustic Oscillations, and Supernovae: Dynamical Dark Energy, Neutrino Masses, Lensing Anomaly, and the Hubble Tension, *Astrophys. J. Lett.* **976**, L11 (2024), arXiv:2409.13022 [astro-ph.CO].
- [49] X. Lu, S. Gao, and Y. Gong, The model-independent evidence of cosmic acceleration revisited, (2024), arXiv:2409.13399 [astro-ph.CO].
- [50] C.-G. Park, J. de Cruz Perez, and B. Ratra, Is the w_0w_a CDM cosmological parameterization evidence for dark energy dynamics partially caused by the excess smoothing of Planck CMB anisotropy data?, (2024), arXiv:2410.13627 [astro-ph.CO].
- [51] T.-N. Li, Y.-H. Li, G.-H. Du, P.-J. Wu, L. Feng, J.-F. Zhang, and X. Zhang, Revisiting holographic dark energy after DESI 2024, (2024), arXiv:2411.08639 [astro-ph.CO].
- [52] G. Payeur, E. McDonough, and R. Brandenberger, Do Observations Prefer Thawing Quintessence?, (2024), arXiv:2411.13637 [astro-ph.CO].
- [53] M. Ishak *et al.*, Modified Gravity Constraints from the Full Shape Modeling of Clustering Measurements from DESI 2024, (2024), arXiv:2411.12026 [astro-ph.CO].
- [54] S. Akthar and M. W. Hossain, General parametrization for energy density of quintessence field, (2024), arXiv:2411.15892 [astro-ph.CO].
- [55] Q. Gao, Z. Peng, S. Gao, and Y. Gong, On the evidence of dynamical dark energy, (2024), arXiv:2411.16046 [astro-ph.CO].
- [56] X. T. Tang, D. Brout, T. Karwal, C. Chang, V. Miranda, and M. Vincenzi, Uniting the Observed Dynamical Dark Energy Preference with the Discrepancies in Ω_m and H_0 Across Cosmological Probes, (2024), arXiv:2412.04430 [astro-ph.CO].
- [57] M. Berbig, Kick it like DESI: PNGB quintessence with a dynamically generated initial velocity, (2024), arXiv:2412.07418 [astro-ph.CO].
- [58] J. de Cruz Perez, C.-G. Park, and B. Ratra, Updated observational constraints on spatially flat and nonflat

- Λ CDM and XCDM cosmological models, *Phys. Rev. D* **110**, 023506 (2024), arXiv:2404.19194 [astro-ph.CO].
- [59] N. Aghanim *et al.* (Planck), Planck 2018 results. VI. Cosmological parameters, *Astron. Astrophys.* **641**, A6 (2020), [Erratum: *Astron. Astrophys.* 652, C4 (2021)], arXiv:1807.06209 [astro-ph.CO].
- [60] J. Solà, A. Gómez-Valent, and J. de Cruz Pérez, Dynamical dark energy: scalar fields and running vacuum, *Mod. Phys. Lett. A* **32**, 1750054 (2017), arXiv:1610.08965 [astro-ph.CO].
- [61] J. Ooba, B. Ratra, and N. Sugiyama, Planck 2015 Constraints on the Nonflat ϕ CDM Inflation Model, *Astrophys. J.* **866**, 68 (2018), arXiv:1712.08617 [astro-ph.CO].
- [62] J. Ooba, B. Ratra, and N. Sugiyama, Planck 2015 constraints on spatially-flat dynamical dark energy models, *Astrophys. Space Sci.* **364**, 176 (2019), arXiv:1802.05571 [astro-ph.CO].
- [63] C.-G. Park and B. Ratra, Observational constraints on the tilted spatially-flat and the untilted nonflat ϕ CDM dynamical dark energy inflation models, *Astrophys. J.* **868**, 83 (2018), arXiv:1807.07421 [astro-ph.CO].
- [64] J. Solà Peracaula, A. Gómez-Valent, and J. de Cruz Pérez, Signs of Dynamical Dark Energy in Current Observations, *Phys. Dark Univ.* **25**, 100311 (2019), arXiv:1811.03505 [astro-ph.CO].
- [65] C.-G. Park and B. Ratra, Using SPT polarization, *Planck* 2015, and non-CMB data to constrain tilted spatially-flat and untilted nonflat Λ CDM, XCDM, and ϕ CDM dark energy inflation cosmologies, *Phys. Rev. D* **101**, 083508 (2020), arXiv:1908.08477 [astro-ph.CO].
- [66] N. Khadka and B. Ratra, Using quasar X-ray and UV flux measurements to constrain cosmological model parameters, *Mon. Not. Roy. Astron. Soc.* **497**, 263 (2020), arXiv:2004.09979 [astro-ph.CO].
- [67] S. Cao, J. Ryan, and B. Ratra, Cosmological constraints from H ii starburst galaxy apparent magnitude and other cosmological measurements, *Mon. Not. Roy. Astron. Soc.* **497**, 3191 (2020), arXiv:2005.12617 [astro-ph.CO].
- [68] N. Khadka and B. Ratra, Constraints on cosmological parameters from gamma-ray burst peak photon energy and bolometric fluence measurements and other data, *Mon. Not. Roy. Astron. Soc.* **499**, 391 (2020), arXiv:2007.13907 [astro-ph.CO].
- [69] S. Cao, J. Ryan, and B. Ratra, Using Pantheon and DES supernova, baryon acoustic oscillation, and Hubble parameter data to constrain the Hubble constant, dark energy dynamics, and spatial curvature, *Mon. Not. Roy. Astron. Soc.* **504**, 300 (2021), arXiv:2101.08817 [astro-ph.CO].
- [70] S. Cao, N. Khadka, and B. Ratra, Standardizing Dainotti-correlated gamma-ray bursts, and using them with standardized Amati-correlated gamma-ray bursts to constrain cosmological model parameters, *Mon. Not. Roy. Astron. Soc.* **510**, 2928 (2022), arXiv:2110.14840 [astro-ph.CO].
- [71] F. Dong, C. Park, S. E. Hong, J. Kim, H. Seong Hwang, H. Park, and S. Appleby, Tomographic Alcock-Paczynski Test with Redshift-space Correlation Function: Evidence for the Dark Energy Equation-of-state Parameter $w > -1$, *Astrophys. J.* **953**, 98 (2023), arXiv:2305.00206 [astro-ph.CO].
- [72] M. Van Raamsdonk and C. Waddell, Suggestions of decreasing dark energy from supernova and BAO data, *JCAP* **06**, 047, arXiv:2305.04946 [astro-ph.CO].
- [73] M. Van Raamsdonk and C. Waddell, Holographic motivations and observational evidence for decreasing dark energy, (2024), arXiv:2406.02688 [hep-th].
- [74] R. I. Thompson, Non-Canonical Dark Energy Parameter Evolution in a Canonical Quintessence Cosmology, *Universe* **10**, 356 (2024), arXiv:2409.06792 [gr-qc].
- [75] E. Calabrese, A. Slosar, A. Melchiorri, G. F. Smoot, and O. Zahn, Cosmic Microwave Weak lensing data as a test for the dark universe, *Phys. Rev. D* **77**, 123531 (2008), arXiv:arXiv:0803.2309 [astro-ph].
- [76] J. de Cruz Pérez, C.-G. Park, and B. Ratra, Current data are consistent with flat spatial hypersurfaces in the Λ CDM cosmological model but favor more lensing than the model predicts, *Phys. Rev. D* **107**, 063522 (2023), arXiv:2211.04268 [astro-ph.CO].
- [77] N. Aghanim *et al.* (Planck), Planck 2018 results. I. Overview and the cosmological legacy of Planck, *Astron. Astrophys.* **641**, A1 (2020), arXiv:1807.06205 [astro-ph.CO].
- [78] D. Brout *et al.*, The Pantheon+ Analysis: Cosmological Constraints, *Astrophys. J.* **938**, 110 (2022), arXiv:2202.04077 [astro-ph.CO].
- [79] S. Cao and B. Ratra, $H_0=69.8\pm 1.3$ km s⁻¹ Mpc⁻¹, $\Omega_{m0}=0.288\pm 0.017$, and other constraints from lower-redshift, non-CMB, expansion-rate data, *Phys. Rev. D* **107**, 103521 (2023), arXiv:2302.14203 [astro-ph.CO].
- [80] A. Challinor and A. Lasenby, Cosmic microwave background anisotropies in the CDM model: A Covariant and gauge invariant approach, *Astrophys. J.* **513**, 1 (1999), arXiv:astro-ph/9804301.
- [81] A. Lewis, A. Challinor, and A. Lasenby, Efficient computation of CMB anisotropies in closed FRW models, *Astrophys. J.* **538**, 473 (2000), arXiv:astro-ph/9911177.
- [82] A. Lewis and S. Bridle, Cosmological parameters from CMB and other data: A Monte Carlo approach, *Phys. Rev. D* **66**, 103511 (2002), arXiv:astro-ph/0205436.
- [83] A. Lewis, GetDist: a Python package for analysing Monte Carlo samples, arXiv:1910.13970 [astro-ph.IM].
- [84] J.-P. Dai, Y. Yang, and J.-Q. Xia, Reconstruction of the Dark Energy Equation of State from the Latest Observations, *Astrophys. J.* **857**, 9 (2018).
- [85] W. Fang, W. Hu, and A. Lewis, Crossing the Phantom Divide with Parameterized Post-Friedmann Dark Energy, *Phys. Rev. D* **78**, 087303 (2008), arXiv:0808.3125 [astro-ph].
- [86] F. Lucchin and S. Matarrese, Power Law Inflation, *Phys. Rev. D* **32**, 1316 (1985).
- [87] B. Ratra, Quantum Mechanics of Exponential Potential Inflation, *Phys. Rev. D* **40**, 3939 (1989).
- [88] B. Ratra, Inflation in an Exponential Potential Scalar Field Model, *Phys. Rev. D* **45**, 1913 (1992).
- [89] S. Joudaki *et al.*, CFHTLenS revisited: assessing concordance with Planck including astrophysical systematics, *Mon. Not. Roy. Astron. Soc.* **465**, 2033 (2017), arXiv:1601.05786 [astro-ph.CO].
- [90] W. Handley and P. Lemos, Quantifying dimensionality: Bayesian cosmological model complexities, *Phys. Rev. D* **100**, 023512 (2019), arXiv:1903.06682.
- [91] W. Handley and P. Lemos, Quantifying tensions in cosmological parameters: Interpreting the DES evidence ratio, *Phys. Rev. D* **100**, 043504 (2019),

- arXiv:1902.04029.
- [92] W. Handley, Curvature tension: evidence for a closed universe, *Phys. Rev. D* **103**, L041301 (2021), arXiv:arXiv:1908.09139 [astro-ph.CO].
- [93] G. Chen and B. Ratra, Median statistics and the Hubble constant, *Publ. Astron. Soc. Pac.* **123**, 1127 (2011), arXiv:1105.5206., arXiv:1105.5206 [astro-ph.CO].
- [94] J. R. Gott, III, M. S. Vogeley, S. Podariu, and B. Ratra, Median statistics, $H(0)$, and the accelerating universe, *Astrophys. J.* **549**, 1 (2001), arXiv:astro-ph/0006103.
- [95] E. Calabrese, M. Archidiacono, A. Melchiorri, and B. Ratra, The impact of a new median statistics H_0 prior on the evidence for dark radiation, *Phys. Rev. D* **86**, 043520 (2012), arXiv:arXiv:1205.6753 [astro-ph.CO].
- [96] W. L. Freedman, B. F. Madore, I. S. Jang, T. J. Hoyt, A. J. Lee, and K. A. Owens, Status Report on the Chicago-Carnegie Hubble Program (CCHP): Three Independent Astrophysical Determinations of the Hubble Constant Using the James Webb Space Telescope, (2024), arXiv:2408.06153 [astro-ph.CO].
- [97] A. G. Riess *et al.*, A Comprehensive Measurement of the Local Value of the Hubble Constant with 1 km/s/Mpc Uncertainty from the Hubble Space Telescope and the SH0ES Team, *Astrophys. J. Lett.* **934**, L7 (2022), arXiv:2112.04510 [astro-ph.CO].
- [98] Y. Chen, S. Kumar, B. Ratra, and T. Xu, Effects of Type Ia Supernovae Absolute Magnitude Priors on the Hubble Constant Value, *Astrophys. J. Lett.* **964**, L4 (2024), arXiv:2401.13187 [astro-ph.CO].
- [99] S. Barua and S. Desai, Effect of Peak Absolute Magnitude of Type Ia Supernovae and Sound Horizon Values on Hubble Tension using DESI results, (2024), arXiv:2412.19240 [astro-ph.CO].
- [100] M. Tristram *et al.*, Cosmological parameters derived from the final Planck data release (PR4), *Astron. Astrophys.* **682**, A37 (2024), arXiv:2309.10034 [astro-ph.CO].
- [101] P. J. E. Peebles and B. Ratra, Cosmology with a Time Variable Cosmological Constant, *Astrophys. J. Lett.* **325**, L17 (1988).
- [102] B. Ratra and P. J. E. Peebles, Cosmological Consequences of a Rolling Homogeneous Scalar Field, *Phys. Rev. D* **37**, 3406 (1988).